JOURNAL OF COMPUTATIONAL PHYSICS 121, 1–28 (1995)

Finite Volume Approximation of Two Phase-Fluid Flows Based on an Approximate Roe-Type Riemann Solver

LIONEL SAINSAULIEU

C.E.R.M.I.C.S., E.N.P.C. Central 2, La Courtine, 93167 Noisy-le-Grand Cedex, France; and Centre de Mathématiques Appliquées, Ecole Polytechnique, 91128 Palaiseau Cedex, France

Received December 11, 1992; revised December 19, 1994

We introduce an approximate Roe type Riemann solver for the numerical simulation of two-phase fluid flows composed of liquid droplets suspended in gas. We compute a Roe linearization of some well-conditioned approximate Rankine–Hugoniot relations in nonconservation form. The computed solutions are found to be in good agreement with the exact solution in one dimension slab geometry. We extend this solver to two-dimensional geometries using a finite volume formulation.

1. INTRODUCTION

We consider a two-phase fluid flow composed of liquid droplets suspended in a gas phase. The droplets are assumed incompressible with constant mass density ρ_l while the gas phase is compressible. The gas flow around the droplets and the liquid flow inside the droplets are respectively governed by compressible and incompressible Navier–Stokes equations. However, clouds of interest typically contain 10^9 to 10^{12} droplets per cubic meter and the free boundary problem cannot be solved. Furthermore, we are not interested in the precise location of droplets but in average quantities. We introduce in [1] an Euler system modeling two-phase fluid flows, where each phase is seen as a fluid described by macroscopic quantities.

We denote by α the volume fraction of the gas phase, ρ_g the gas mass density, ρ_l the liquid phase mass density, $\mathbf{u}_g$ and $\mathbf{u}_l$ the average gas and liquid phase velocities, and by ε_g and ε_l the specific internal energies of the gas and liquid phases, respectively.

Remark 1.1. For two phase flows of interest, the mass density ρ_l of the liquid phase is very large in comparison with the gas mass density ρ_g. In cryogenic engines, for instance, the liquid oxygen and gaseous hydrogen are injected in the engine in proportions close to stoichiometry. Hence the liquid phase volume fraction $1 - \alpha$ is of order ρ_g/ρ_l. We restrict, hereafter, ourselves to this situation.

The macroscopic Euler system that describes the flow is obtained by averaging the Navier–Stokes equations governing the flow at the microscopic scale. This procedure described in [1] relies in particular on the assumption that the volume fraction α is close to 1. Omitting the mass, impulsion, and energy algebraic exchange terms between the two phases, the system obtained in [1] reads:

$$\partial_t(\alpha\rho_g) + \nabla\cdot(\alpha\rho_g\mathbf{u}_g) = 0 \tag{1.1.i}$$

$$\partial_t(\alpha\rho_g\mathbf{u}_g) + \nabla\cdot(\alpha\rho_g(\mathbf{u}_g\otimes\mathbf{u}_g)) + \alpha\nabla p - \nabla\cdot\sigma_g' = \mathbf{0} \tag{1.1.ii}$$

$$\partial_t(\alpha\rho_g e_g) + \nabla\cdot(\alpha\rho_g e_g\mathbf{u}_g + \alpha p\mathbf{u}_g) + p\nabla\cdot((1-\alpha)\mathbf{u}_l) - \nabla\cdot(\sigma_g'\mathbf{u}_g) - \nabla\cdot(\kappa_g\nabla\varepsilon_g) = 0 \tag{1.1.iii}$$

$$\partial_t((1-\alpha)\rho_l) + \nabla\cdot((1-\alpha)\rho_l\mathbf{u}_l) = 0 \tag{1.1.iv}$$

$$\partial_t((1-\alpha)\rho_l\mathbf{u}_l) + \nabla\cdot((1-\alpha)\rho_l(\mathbf{u}_l\otimes\mathbf{u}_l)) + (1-\alpha)\nabla p + \nabla\theta - \nabla\cdot\sigma_l' = \mathbf{0} \tag{1.1.v}$$

$$\partial_t((1-\alpha)\rho_l e_l) + \nabla\cdot((1-\alpha)\rho_l e_l\mathbf{u}_l) + (1-\alpha)\mathbf{u}_l\cdot\nabla p + \nabla\cdot(\theta\mathbf{u}_l) - \nabla\cdot(\sigma_l'\mathbf{u}_l) = 0. \tag{1.1.vi}$$

We have written the mass, impulsion, and energy conservation equations for the gas phase and the liquid phase. The gas and liquid phase specific total energies are

$$e_g = \varepsilon_g + u_g^2/2, \quad e_l = \varepsilon_l + u_l^2/2$$

while the pressures p and θ are defined by

$$p = (\gamma - 1)\rho_g\varepsilon_g, \quad \theta = \theta_0(1-\alpha)^\delta.$$

The constant θ_0 is proportional to the rest pressure of the gas flow on the droplets. We take $\theta_0 = 10000$ *Pascal* in the sequel. For two phase flows, we obtain that the exponent δ is $\delta = \frac{4}{3}$. Finally the viscous stress tensors σ_g' and σ_l' of the gas and liquid phases are defined by

$$\sigma_g' = \eta_g(\nabla\mathbf{u}_g + \nabla\mathbf{u}_g^{\mathrm{T}}) + (\zeta_g^0 - \tfrac{2}{3}\eta_g)(\nabla\cdot\mathbf{u}_g)\mathbf{1},$$

0021-9991/95 $12.00

and

$$\sigma_l' = \eta_l(\nabla \mathbf{u}_l + \nabla \mathbf{u}_l^T),$$

where $\eta_g = \eta_g^0(1 + 5(1 - \alpha)/2)$ is the effective shear viscosity coefficient of the gas and η_l is an effective viscosity coefficient for the dispersed phase (distinct from the viscosity of the liquid), taken as a constant. Here η_g^0 and ξ_g^0 denote respectively the shear and bulk viscosity coefficients of the gas and $\kappa_g = \kappa_g^0\alpha$ is the thermal conduction of the two-phase flow. Usually coefficient η_l is much smaller than η_g.

The impulsion and energy equations in system (1.1) are written in nonconservation form. Note, however, that the total impulsion and total energy equations are in conservation form.

We study system (1.1) in one-dimensional slab geometry in [2, 3]. We denote by $\mathbf{u}$ the state vector:

$$\mathbf{u}^T = (\alpha\rho_g, \alpha\rho_g u_g, \alpha\rho_g e_g, (1 - \alpha)\rho_l, (1 - \alpha)\rho_l u_l, (1 - \alpha)\rho_l e_l).$$

We denote next by Ω the set of the physical states:

$$\Omega = \{\mathbf{u} \in \mathbb{R}^6, \rho_g > 0, 0 \leq \alpha \leq 1, \varepsilon_g > 0, \varepsilon_l > 0\}.$$

In one-dimensional slab geometry, system (1.1) takes the condensed form

$$\partial_t \mathbf{u} + \mathbf{A}(\mathbf{u})\,\partial_x \mathbf{u} - \partial_x(\mathbf{D}(\mathbf{u})\,\partial_x \mathbf{u}) = \mathbf{0} \tag{1.2}$$

and the convection terms extracted from (1.2) read

$$\partial_t \mathbf{u} + \mathbf{A}(\mathbf{u})\,\partial_x \mathbf{u} = \mathbf{0}. \tag{1.3}$$

We prove in [2] that for some positive real numbers ε and M, system (1.3) is strictly hyperbolic over the set Ω_ε^M defined by

$$\Omega_\varepsilon^M = \{\mathbf{u} \in \Omega, 0 < 1 - \alpha < \varepsilon, |u_g - u_l| \leq (1 - \varepsilon)c_g, |\mathbf{u}| \leq M\},$$

where c_g is the gas sound speed: $c_g = \sqrt{\gamma p/\rho_g}$; for any $\mathbf{u} \in \Omega_\varepsilon^M$, matrix $\mathbf{A}(\mathbf{u})$ has six real eigenvalues and can be diagonalized over $\mathbb{R}$. We compute the following expansion in $1 - \alpha$ of the eigenvalues of $\mathbf{A}(\mathbf{u})$:

$$\begin{aligned}
\lambda_1 &= u_g - c_g + o((1 - \alpha)^{\delta-1}) \\
\lambda_2 &= u_g + c_g + o((1 - \alpha)^{\delta-1}) \\
\lambda_3 &= u_l - \left(\frac{-\theta'(\alpha)}{\rho_l}\right)^{1/2} + o((1 - \alpha)^{(\delta-1)/2}) \\
\lambda_4 &= u_l + \left(\frac{-\theta'(\alpha)}{\rho_l}\right)^{1/2} + o((1 - \alpha)^{(\delta-1)/2}) \\
\lambda_5 &= u_g \\
\lambda_6 &= u_l.
\end{aligned} \tag{1.4}$$

Remark 1.2. The pressure correction θ is small in comparison with the gas pressure p. It plays, however, an important role from the mathematical viewpoint since matrix $\mathbf{A}(\mathbf{u})$ would have complex eigenvalues even for α close to 1 if we had omitted it. The initial value problem for (1.3) would be ill-posed. The presence of the pressure correction θ gives a hyperbolic system.

The diffusion coefficients in system (1.2) are small and we want to avoid solving the small scale effects connected with the diffusion by considering the convection system (1.3) extracted from (1.2). In the same manner as in the case of *conservative* hyperbolic system, we expect the formation of shock in solutions of (1.3) even for smooth initial data. But when $\mathbf{u}$ is a discontinuous function, the product $\mathbf{A}(\mathbf{u})\partial_x \mathbf{u}$ has no meaning as a distribution. To define shock waves solution of (1.3), we have to add some extra information to system (1.3). Recalling that (1.3) is extracted from (1.2), we define in [2] the shock waves solution of (1.3) as the limit when the diffusion is neglected of traveling waves solution of (1.2): let $\mathbf{u}(x, t) = \hat{\mathbf{u}}(x - \sigma t)$ denote a traveling wave with speed σ solution of (1.2). Then,

$$-\sigma\hat{\mathbf{u}}' + \mathbf{A}(\hat{\mathbf{u}})\hat{\mathbf{u}}' - (\mathbf{D}(\hat{\mathbf{u}})\hat{\mathbf{u}}')' = \mathbf{0}.$$

Denote by $\mathbf{u}^L$ and $\mathbf{u}^R$ the left and right states connected by $\mathbf{u}$:

$$\lim_{\xi \to -\infty} \mathbf{u}(x, t) = \mathbf{u}^L, \quad \lim_{\xi \to +\infty} \mathbf{u}(\xi) = \mathbf{u}^R.$$

For $\varepsilon > 0$, set

$$\mathbf{u}_\varepsilon(x, t) = \hat{\mathbf{u}}\left(\frac{x - \sigma t}{\varepsilon}\right).$$

Function $\mathbf{u}_\varepsilon$ is a traveling wave with speed σ solution of

$$\partial_t \mathbf{u}_\varepsilon + \mathbf{A}(\mathbf{u}_\varepsilon)\,\partial_x \mathbf{u}_\varepsilon - \partial_x(\varepsilon\mathbf{D}(\mathbf{u}_\varepsilon)\,\partial_x \mathbf{u}_\varepsilon) = \mathbf{0}.$$

Furthermore, when ε tends to zero, function $\mathbf{u}_\varepsilon$ converges a.e. to the discontinuous function

$$\mathbf{u}_0(x, t) = \begin{cases} \mathbf{u}^L & \text{if } x < \sigma t \\ \mathbf{u}^R & \text{if } x > \sigma t. \end{cases} \tag{1.5}$$

DEFINITION AND PROPOSITION 1.1. Let $\mathbf{u}(x, t) = \hat{\mathbf{u}}(x - \sigma t)$ be a traveling wave with speed σ solution of (1.2). We say that function $\mathbf{u}_0$ defined by (1.5) is a shock wave with speed σ solution of (1.3), which is compatible with the diffusion tensor $\mathbf{D}$. It satisfies the jump conditions:

$$\sigma(\mathbf{u}^R - \mathbf{u}^L) = \int_{-\infty}^{+\infty} \mathbf{A}(\hat{\mathbf{u}}(\xi))\hat{\mathbf{u}}'(\xi)\,d\xi. \tag{1.6}$$

Definition 1.1 of the shock waves depends on the shape of the diffusion tensor $\mathbf{D}$ in the convection-diffusion system (1.2)

from which system (1.3) is extracted; for instance, we obtain that when the viscosity coefficient η_l in $\mathbf{D}$ is set to zero, system (1.2) is equivalent with a system in conservation form. On the contrary when η_l is non-zero no equivalent conservation form is known.

Here the choice of the diffusion tensor $\mathbf{D}$ requires further attention. First when η_l is set to zero, a straightforward computation (see [2]) shows that the continuous traveling waves solution of (1, 2) are solution of the system in conservation form:

$$\partial_t(\alpha\rho_g + (1-\alpha)\rho_l) + \partial_x(\alpha\rho_g u_g + (1-\alpha)\rho_l u_l) = 0 \quad (1.7.\text{i})$$

$$\partial_t(\alpha\rho_g u_g + (1-\alpha)\rho_l u_l) + \partial_x(\alpha\rho_g u_g^2 + (1-\alpha)\rho_l u_l^2) + \partial_x(p+\theta) - \partial_x(\eta_g \partial_x u_g) = 0 \quad (1.7.\text{ii})$$

$$\partial_t(\alpha\rho_g e_g + (1-\alpha)\rho_l e_l) + \partial_x(\alpha\rho_g e_g u_g + (1-\alpha)\rho_l e_l u_l) + \partial_x(p(\alpha u_g + (1-\alpha)u_l)) + \partial_x(\theta u_l) - \partial_x(\eta_g u_g\, \partial x u_g) - \partial_x(\kappa_g \partial_x \varepsilon_g) = 0 \quad (1.7.\text{iii})$$

$$\partial_t((1-\alpha)\rho_l) + \partial_x((1-\alpha)\rho_l u_l) = 0 \quad (1.7.\text{iv})$$

$$\partial_t(u_l) + \partial_x\left(\frac{u_l^2}{2} + \frac{p}{\rho_l} + \frac{\delta\theta_0}{\rho_l(\delta-1)}(1-\alpha)^{\delta-1}\right) = 0 \quad (1.7.\text{v})$$

$$\partial_t((1-\alpha)\rho_l\varepsilon_l^e) + \partial_x((1-\alpha)\rho_l\varepsilon_l^e u_l) = 0 \quad (1.7.\text{vi})$$

where

$$\varepsilon_l^e = \varepsilon - \frac{\delta\theta_0}{\rho_l(\delta-1)}(1-\alpha)^{\delta-1}. \quad (1.8)$$

When $\eta_l = 0$, the shock waves solution of (1.2) that are compatible with the diffusion tensor $\mathbf{D}$ are the admissible shock waves solution of the first-order hyperbolic system extracted from (1.7). The jump conditions (1.6) are then explicit and in conservation form. Indeed, denote by $\mathbf{w}$ the dependent variables:

$$\mathbf{w}^{\mathrm{T}} = (\alpha\rho_g + (1-\alpha)\rho_l, \alpha\rho_g u_g + (1-\alpha)\rho_l u_l, \alpha\rho_g e_g + (1-\alpha)\rho_l e_l, (1-\alpha)\rho_l, u_l, (1-\alpha)\rho_l\varepsilon_l^e). \quad (1.9)$$

Write next the first-order system in conservation form extracted from (1.7) as

$$\partial_t \mathbf{w} + \partial_x \mathbf{g}(\mathbf{w}) = \mathbf{0} \quad (1.10)$$

for some appropriate flux function $\mathbf{g}$. Then the jump conditions (1.6) are equivalent with

$$\sigma(\mathbf{w}^R - \mathbf{w}^L) = \mathbf{g}(\mathbf{w}^R) - \mathbf{g}(\mathbf{w}^L). \quad (1.11)$$

The viscosity coefficient η_l is very small in comparison with η_g and we are tempted to use system (1.7) rather than (1.2). However, this is only possible for very weak shocks. Indeed, the equivalence between (1.2) (in 1D slab geometry) and (1.7) holds only for continuous solutions. But let be given $\mathbf{u}^L, \mathbf{u}^R \in \Omega_\varepsilon^M$ and $\sigma \in \mathbb{R}$ that satisfy the jump conditions (1.11). When σ is in closed from $\lambda_3(\mathbf{u}^L)$, we prove in [4] that we can obtain a continuous traveling wave with speed σ that connects $\mathbf{w}^L$ and $\mathbf{w}^R$ and a solution of (1.7) only if $|\mathbf{w}^R - \mathbf{w}^L|$ is very small. When the left and right states are more distant, no continuous solution of (1.7) exists. Hence, the equivalence of systems (1.2) and (1.7) only holds for very weak shocks. This prevents considering (1.2) and (1.7) equivalent in applications.

When η_l is small but nonzero, we can construct traveling wave solutions of (1.2) that connect distant left and right states. This solution is very close to a continuous traveling wave solution of (1.7) only when the left and right states connected by the wave are very close to one another. (See [4] for more details and Section 2 below for the sketch of the construction of solutions.)

Finally for shock waves of interest, the viscosity coefficient η_l cannot be neglected and no equivalent conservation form of system (1.2) is available. We sketch in Section 2 the construction of some traveling wave solutions of (1.2) and we deduce some approximate jump conditions for the shock wave solutions of (1.3). These approximate jump conditions are written in nonconservation form. We write in Section 3 a Roe-type solver based on a Roe linearization of these latter jump conditions. Sections 4 and 5 are devoted to numerical results in one and two space dimensions. In the case of one-dimensional slab geometry we compare our results with results obtained with two other numerical methods, described in [5, 6].

2. APPROXIMATE RANKINE–HUGONIOT RELATIONS

The jump conditions (1.6) depend upon the viscous profile associated with the shock wave. Needing explicit jump conditions for computations we need more information on this profile and we sketch the construction of the traveling wave solution of (1.2) by a method of successive approximations.

Recall that for two-phase fluid flows of interest, the volume fraction $1-\alpha$ of the liquid phase is of the same order as the small quotient ρ_g/ρ_l. Then, system (1.2) consists of two systems in conservation form, weakly coupled by small terms in nonconservation form; this follows from the adimensionalization of the system (1.2). Denote by ρ_g^* and ε_g^* the reference gas mass density and gas specific internal energy, respectively. Write next

$$\rho_g = \rho_g^*\tilde{\rho}_g, \quad \varepsilon_g = \varepsilon_g^*\tilde{\varepsilon}_g, \quad u_g = \sqrt{\varepsilon_g^*}\tilde{u}_g$$

$$(1-\alpha)\rho_l = \rho_g^*\tilde{\beta}, \quad \varepsilon_l = \varepsilon_g^*\tilde{\varepsilon}_l, \quad u_l = \sqrt{\varepsilon_g^*}\tilde{u}_l.$$

Then, the gas pressure p is given by

$$p = (\gamma-1)\rho_g\varepsilon_g = (\gamma-1)\rho_g^*\varepsilon_g^*\tilde{\rho}_g\tilde{\varepsilon}_g = \rho_g^*\varepsilon_g^*\tilde{p}.$$

Define next the coordinate ξ by

$$\xi = x/\sqrt{\varepsilon_g^*}.$$

Then, if $\mathbf{u}$ is a solution of (1.2), the vector valued function $\mathbf{v}$, defined by

$$\begin{aligned}\mathbf{v}^{\mathrm{T}} &= ((\alpha\tilde{\rho}_g, \alpha\tilde{\rho}_g\tilde{u}_g, \alpha\tilde{\rho}_g\tilde{e}_g), (\tilde{\beta}, \tilde{\beta}\tilde{u}_l, \tilde{\beta}\tilde{e}_l))\\ &= (\mathbf{v}_1, \mathbf{v}_2)^{\mathrm{T}},\end{aligned}$$

where $\tilde{e}_g = \tilde{\varepsilon}_g + \tilde{u}_g^2/2$ and $\tilde{e}_l = \tilde{\varepsilon}_l + \tilde{u}_l^2/2$ is a solution of the system of equations

$$\partial_t(\alpha\tilde{\rho}_g) + \partial_\xi(\alpha\tilde{\rho}_g\tilde{u}_g) = 0 \tag{2.1.i}$$

$$\partial_t(\alpha\tilde{\rho}_g\tilde{u}_g) + \partial_\xi(\alpha\tilde{\rho}_g\tilde{u}_g^2) + \partial_\xi(\alpha\tilde{p}) - \partial_\xi\left(\frac{\mu_g}{\rho_g^*\varepsilon_g^*}\partial_\xi\tilde{u}_g\right) = -\varepsilon\alpha\tilde{p}\frac{\partial_\xi\tilde{\beta}}{1-\varepsilon\tilde{\beta}} \tag{2.1.ii}$$

$$\partial_t(\alpha\tilde{\rho}_g\tilde{e}_g) + \partial_\xi(\alpha\tilde{\rho}_g\tilde{e}_g\tilde{u}_g) + \partial_\xi(\alpha\tilde{p}\tilde{u}_g) - \partial_\xi\left(\frac{\mu_g}{\rho_g^*\varepsilon_g^*}\tilde{u}_g\,\partial_\xi\tilde{u}_g\right) - \partial_\xi\left(\frac{\kappa_g}{\rho_g^*\varepsilon_g^*}\partial_\xi\tilde{\varepsilon}_g\right) = -\varepsilon\alpha\tilde{p}\frac{\partial_\xi(\tilde{\beta}\tilde{u}_l)}{1-\varepsilon\tilde{\beta}} \tag{2.1.iii}$$

$$\partial_t\tilde{\beta} + \partial_\xi(\tilde{\beta}\tilde{u}_l) = 0 \tag{2.1.iv}$$

$$\partial_t\tilde{\beta}\tilde{u}_l + \partial_\xi(\tilde{\beta}\tilde{u}_l^2) + \theta_l\partial_\xi(\tilde{\beta}^\delta) - \partial_\xi\left(\frac{\eta_l}{\rho_g^*\varepsilon_g^*}\partial_\xi\tilde{u}_l\right) = -\varepsilon\tilde{\beta}\,\partial_\xi\left(\frac{\alpha\tilde{p}}{1-\varepsilon\tilde{\beta}}\right) \tag{2.1.v}$$

$$\partial_t(\tilde{\beta}\tilde{e}_l) + \partial_\xi(\tilde{\beta}\tilde{e}_l\tilde{u}_l) + \partial_\xi(\theta_1\tilde{\beta}^\delta\tilde{u}_l) - \partial_\xi\left(\frac{\eta_l}{\rho_g^*\varepsilon_g^*}\tilde{u}_l\partial_\xi\tilde{u}_l\right) = -\varepsilon\tilde{\beta}\tilde{u}_l\,\partial_\xi\left(\frac{\alpha\tilde{p}}{1-\varepsilon\tilde{\beta}}\right), \tag{2.1.vi}$$

where we have set

$$\varepsilon = \frac{\rho_g^*}{\rho_l}, \quad \theta_1 = \varepsilon^\delta\theta_0.$$

In condensed form, the system (2.1) is written

$$\partial_t\mathbf{v}_1 + \partial_\xi\mathbf{g}_1(\mathbf{v}_1) - \partial_\xi(\mathbf{D}_1(\mathbf{v}_1)\partial_\xi\mathbf{v}_1) = \varepsilon\mathbf{B}_1(\mathbf{v})\,\partial_\xi\mathbf{v} \tag{2.2.i}$$

$$\partial_t\mathbf{v}_2 + \partial_\xi\mathbf{g}_2(\mathbf{v}_2) - \partial_\xi(\mathbf{D}_2(\mathbf{v}_2)\,\partial_\xi\mathbf{v}_2) = \varepsilon\mathbf{B}_2(\mathbf{v})\,\partial_\xi\mathbf{v}. \tag{2.2.ii}$$

When ε is set to zero, the system (2.2) reads

$$\partial_t\mathbf{v}_1 + \partial_x\mathbf{g}_1(\mathbf{v}_1) - \partial_x(\mathbf{D}_1(\mathbf{v}_1)\,\partial_x\mathbf{v}_1) = 0 \tag{2.3.i}$$

$$\partial_t\mathbf{v}_2 + \partial_x\mathbf{g}_2(\mathbf{v}_2) - \partial_x(\mathbf{D}_2(\mathbf{v}_2)\,\partial_x\mathbf{v}_2) = 0. \tag{2.3.ii}$$

The system (2.3) is made of two decoupled subsystems; the first one is the set of Navier–Stokes equations in one space dimension. Its solutions are studied in [7, 8]. The second subsystem is a convection–diffusion system of the same type.

Let $\mathbf{v}_1^0$ be a traveling wave with speed σ solution of (2.3.i) and let it be given a state $\mathbf{v}_2^L$. Then the function

$$\mathbf{v}(\xi) = (\mathbf{v}_1(\xi), \mathbf{v}_2^L)$$

is a traveling wave with speed σ solution of (2.3). In the same manner, if $\mathbf{v}_2$ is a traveling wave with speed σ solution of (2.3.ii) and $\mathbf{v}_1^L$ is a given state, we obtain a traveling wave with speed σ solution of (2.3) as

$$\mathbf{v}(\xi) = (\mathbf{v}_1^L, \mathbf{v}_2(\xi)).$$

We assume next that the number ε is small and that the number θ_l is of order 0 in ε. The solutions of (2.2) are obtained as perturbations of the solutions of (2.3).

THEOREM 2.1. *Let it be given that $\mathbf{v}^0 = (\mathbf{v}_1^0, \mathbf{v}_2^0)$, a traveling wave with speed σ solution of* (2.3) *such that either $\mathbf{v}_1^0$ is a traveling wave with speed σ solution of* (2.3.*i*) *and $\mathbf{v}_2^0$ is a constant function, or $\mathbf{v}_1^0$ is a constant function and $\mathbf{v}_2^0$ is a traveling wave with speed σ solution of* (2.3.*ii*). *Set $\mathbf{v}^L = (\mathbf{v}_1^L, \mathbf{v}_2^L) = \mathbf{v}^0(-\infty)$. Then, for ε small enough, the successive approximations*

$$-\sigma(\mathbf{v}_1^{p+1} - \mathbf{v}_1^L) + \mathbf{g}_1(\mathbf{v}_1^{p+1}) - \mathbf{g}_1(\mathbf{v}_1^L) - \mathbf{D}_1(\mathbf{v}_1^{p+1})'(\mathbf{v}_1^{p+1})' = \varepsilon\int_{-\infty}^{x}\mathbf{B}_1(\mathbf{v}^p)(\mathbf{v}^p)'\,ds \tag{2.4.i}$$

$$-\sigma(\mathbf{v}_2^{p+1} - \mathbf{v}_2^L) + \mathbf{g}_2(\mathbf{v}_2^{p+1}) - \mathbf{g}_2(\mathbf{v}_2^L) - \mathbf{D}_2(\mathbf{v}_2^{p+1})(\mathbf{v}_2^{p+1})' = \varepsilon\int_{-\infty}^{x}\mathbf{B}_2(\mathbf{v}^p)(\mathbf{v}^p)'\,ds \tag{2.4.ii}$$

define a sequence $\mathbf{v}^p$, $p \geq 0$, with $\mathbf{v}^p(-\infty) = \mathbf{v}^0(-\infty)$. This sequence converges when p tends to $+\infty$ to a traveling wave $\mathbf{v}$ with speed σ and $\mathbf{v}(-\infty) = \mathbf{v}^L$, solution of (2.3). *Furthermore, $\mathbf{v}$ satisfies the following approximate jump conditions:*

$$\begin{aligned}[\alpha\tilde{\rho}_g(\tilde{u}_g - \sigma)] &= 0\\ [\alpha\tilde{\rho}_g\tilde{u}_g(\tilde{u}_g - \sigma)] + [\alpha\tilde{p}] - \alpha^L\tilde{p}^L[\log(1-\varepsilon\tilde{\beta})] &= O(\varepsilon^2)\\ [\alpha\tilde{\rho}_g\tilde{e}_g(\tilde{u}_g - \sigma)] + [\alpha\tilde{p}\tilde{u}_g] - \sigma\alpha^L\tilde{p}^L[\log(1-\varepsilon\tilde{\beta})] &= O(\varepsilon^2)\\ [\tilde{\beta}(\tilde{u}_l - \sigma)] &= 0\end{aligned} \tag{2.5.i}$$

$$\left[\tilde{\beta}\tilde{u}_l(\tilde{u}_l - \sigma) + \theta_1\tilde{\beta}^\delta + \varepsilon\frac{\alpha\tilde{p}\tilde{\beta}}{1-\varepsilon\tilde{\beta}}\right] + \alpha^L\tilde{p}^L[\log(1-\varepsilon\tilde{\beta})] = O(\varepsilon^2)$$

$$[\tilde{\beta}\tilde{e}_l(\tilde{u}_l - \sigma) + \theta_1\tilde{\beta}^\delta\tilde{u}_l + \sigma\alpha^L\tilde{p}^L[\log(1-\varepsilon\tilde{\beta})] = O(\varepsilon^2). \quad (2.5.ii)$$

Proof. We prove in [8] that for ε small enough, (2.4) defines a sequence $\mathbf{v}^p$, $p \geq 0$, that converges to a solution of (2.2). Furthermore,

$$\|(\mathbf{v} - \mathbf{v}^0)'\|_{L^1(\mathbf{R})} \leq C\varepsilon \quad (2.6)$$

for some positive number C. Inserting this latter estimate in (2.2) gives the approximate jump conditions:

$$-\sigma(\mathbf{v}_1(+\infty) - \mathbf{v}_1(-\infty)) + \mathbf{g}_1(\mathbf{v}_1(+\infty)) - \mathbf{g}_1(\mathbf{v}_1(-\infty)) = \varepsilon\int_{-\infty}^{+\infty}\mathbf{B}_1(\mathbf{v}^0)(\mathbf{v}^0)'\,ds + O(\varepsilon^2) \quad (2.7.i)$$

$$-\sigma(\mathbf{v}_2(+\infty) - \mathbf{v}_2(-\infty)) + \mathbf{g}_2(\mathbf{v}_2(+\infty)) - \mathbf{g}_2(\mathbf{v}_2(-\infty)) = \varepsilon\int_{-\infty}^{+\infty}\mathbf{B}_2(\mathbf{v}^0)(\mathbf{v}^0)'\,ds + O(\varepsilon^2). \quad (2.7.ii)$$

But either function $\mathbf{v}_1^0$ or function $\mathbf{v}_2^0$ is constant. When $\mathbf{v}_1^0$ is constant, we compute, for instance,

$$\int_{-\infty}^{+\infty}\alpha^0\tilde{p}^0\left(\frac{\tilde{\beta}^0}{1-\varepsilon\tilde{\beta}^0}\right)'ds = \alpha^L\tilde{p}^L[\log(1-\varepsilon\tilde{\beta}^0)].$$

On the contrary, when $\mathbf{v}_2^0$ is constant, we have

$$\int_{-\infty}^{+\infty}\alpha^0\tilde{p}^0\left(\frac{\tilde{\beta}^0}{1-\varepsilon\tilde{\beta}^0}\right)'ds = 0$$

and

$$\alpha^L\tilde{p}^L[\log(1-\varepsilon\tilde{\beta}^0)] = 0.$$

Using (2.6), we can write in both cases

$$\int_{-\infty}^{+\infty}\alpha^0\tilde{p}^0\left(\frac{\tilde{\beta}}{1-\varepsilon\tilde{\beta}}\right)'ds = \alpha^L\tilde{p}^L[\log(1-\varepsilon\tilde{\beta}^0)] = \alpha^L\tilde{p}^L[\log(1-\varepsilon\tilde{\beta})] + O(\varepsilon^2).$$

This concludes the proof of Theorem 2.1. ∎

Returning to the system of variables $\mathbf{u}$, we obtain with Theorem 2.1 traveling waves solutions of (1.2) that satisfy the approximate jump conditions:

$$\begin{aligned}
[\alpha\rho_g(u_g - \sigma)] &= 0\\
[\alpha\rho_g u_g(u_g - \sigma)] + [\alpha p] - \alpha^L p^L[\log(\alpha)] &= O(\varepsilon^2)\\
[\alpha\rho_g e_g(u_g - \sigma)] + [\alpha p u_g] - \sigma\alpha^L p^L[\log(\alpha)] &= O(\varepsilon^2) \quad (2.8.i)\\
[(1-\alpha)\rho_l(u_l - \sigma)] &= 0\\
[(1-\alpha)\rho_l u_l(u_l - \sigma)] + [\theta_0(1-\alpha)^\delta] + [p(1-\alpha)] + \alpha^L p^L[\log(\alpha)] &= O(\varepsilon^2)\\
[(1-\alpha)\rho_l e_l(u_l - \sigma)] + [\theta_0(1-\alpha)^\delta u_l] + [pu_l(1-\alpha)] + \sigma\alpha^L p^L[\log(\alpha)] &= O(\varepsilon^2). \quad (2.8.ii)
\end{aligned}$$

Remark 2.1. Note that these jump relations are written in nonconservation form. Furthermore, they are perturbations of order ε of the decoupled jump relations in conservation form:

$$\begin{aligned}
[\alpha\rho_g(u_g - \sigma)] &= 0\\
[\alpha\rho_g u_g(u_g - \sigma)] + [\alpha p] &= 0\\
[\alpha\rho_g e_g(u_g - \sigma)] + [\alpha p u_g] &= 0 \quad (2.9.i)\\
[(1-\alpha)\rho_l(u_l - \sigma)] &= 0\\
[(1-\alpha)\rho_l u_l(u_l - \sigma)] + [\theta_0(1-\alpha)^\delta] &= 0\\
[(1-\alpha)\rho_l e_l(u_l - \sigma)] + [\theta_0(1-\alpha)^\delta u_l] &= 0. \quad (2.9.ii)
\end{aligned}$$

Let us give two examples of shock wave solutions of (1.3) that satisfy the approximate jump conditions (2.8): first a solution close to a shock wave solution of the Euler system of gas dynamics (see Table I).

This shock wave with speed $\sigma = 110$ ms^{-1} is referred to as shock wave 1 in the sequel. For this wave, the quantities associated with the liquid phase remain almost constant.

Second we give an example of a shock wave that satisfies the approximate jump conditions (2.8) and that is close to a shock wave solution of the hyperbolic system (see Table II):

$$\begin{aligned}
\partial(1-\alpha)\rho_l + \partial_x(1-\alpha)\rho_l u_l &= 0\\
\partial(1-\alpha)\rho_l u_l + \partial_x(1-\alpha)\rho_l u_l^2 + \partial_x\theta_0(1-\alpha)^\delta &= 0 \quad (2.10)\\
\partial(1-\alpha)\rho_l e_l + \partial_x(1-\alpha)\rho_l e_l u_l + \partial_x\theta_0(1-\alpha)^\delta u_l &= 0.
\end{aligned}$$

This shock wave with speed $\sigma = 23.119$ ms^{-1} is referred to as shock wave 2 in the sequel. This wave mainly affects the quantities associated with the liquid phase.

TABLE I

	ρ_g	α	u_g	u_l	T_g	T_l
$\mathbf{u}^L$	1.0000	0.9900000	−100.	−150.	300.000	300.00
$\mathbf{u}^R$	0.4097	0.9900094	−402.583	−150.244	190.998	299.99

TABLE II

	ρ_g	α	u_g	u_l	T_g	T_l
$\mathbf{u}^L$	0.99776	.95	103.416	22.495	299.732	300.01
$\mathbf{u}^R$	1.00000	.99	100.000	20.000	300.00	300.00

3. ROE-TYPE RIEMANN SOLVER

The Roe-type numerical scheme we introduce below relies on a linearization of the approximate jump conditions (2.8) under the form

$$\tilde{\mathbf{A}}(\mathbf{u}^L, \mathbf{u}^R)(\mathbf{u}^R - \mathbf{u}^L) = \sigma(\mathbf{u}^R - \mathbf{u}^L), \tag{3.1}$$

where the matrix valued function $(\mathbf{u}^L, \mathbf{u}^R) \to \tilde{\mathbf{A}}(\mathbf{u}^L, \mathbf{u}^R)$ is chosen so that (3.1) and (2.8) are equivalent. Recall that the parameter ε is small: we obtain our Roe linearization of conditions (2.8) as a perturbation of a linearization of conditions (2.9). We first write a linearization of (2.9).

LEMMA 3.1. *Let be given two states* $\mathbf{u}^L$ *and* $\mathbf{u}^R$. *We define the average quantities* $\overline{\alpha\rho_g}$, $\overline{u}_g$, $\overline{\varepsilon}_g$, $\overline{1-\alpha}$, $\overline{u}_l$ *and* $\overline{\varepsilon}_l$ *by*

$$\begin{aligned}
\overline{\alpha\rho_g}^{1/2} &= \frac{(\alpha^L\rho_g^L)^{1/2} + (\alpha^R\rho_g^R)^{1/2}}{2},\\
\overline{u}_g &= \frac{(\alpha^L\rho_g^L)^{1/2}u_g^L + (\alpha^R\rho_g^R)^{1/2}u_g^R}{(\alpha^L\rho_g^L)^{1/2} + (\alpha^R\rho_g^R)^{1/2}},\\
\overline{h}_g &= \frac{(\alpha^L\rho_g^L)^{1/2}h_g^L + (\alpha^R\rho_g^R)^{1/2}h_g^R}{(\alpha^L\rho_g^L)^{1/2} + (\alpha^R\rho_g^R)^{1/2}},\\
\overline{\varepsilon}_g &= \frac{1}{\gamma}\left(\overline{h}_g - \frac{\overline{u}_g^2}{2}\right),
\end{aligned} \tag{3.2.i}$$

where

$$h_g = e_g + \frac{p}{\rho_g} = \gamma\varepsilon_g + \frac{1}{2}u_g^2$$

is the gas specific enthalpy and

$$\begin{aligned}
\overline{1-\alpha}^{1/2} &= \frac{(1-\alpha^L)^{1/2} + (1-\alpha^R)^{1/2}}{2}\\
\overline{u}_l &= \frac{(1-\alpha^L)^{1/2}u_l^L + (1-\alpha^R)^{1/2}u_l^R}{(1-\alpha^L)^{1/2} + (1-\alpha^R)^{1/2}},\\
\overline{e}_l &= \frac{(1-\alpha^L)^{1/2}e_l^L + (1-\alpha^R)^{1/2}e_l^R}{(1-\alpha^L)^{1/2} + (1-\alpha^R)^{1/2}}.
\end{aligned} \tag{3.2.ii}$$

Matrix $\mathbf{A}_{11}^0$ *defined by*

$$\mathbf{A}_{11}^0(\mathbf{u}^L, \mathbf{u}^R) = \begin{pmatrix} 0 & 1 & 0\\ -\frac{3-\gamma}{2}\overline{u}_g^2 & (3-\gamma)\overline{u}_g & \gamma-1\\ -\gamma\overline{\varepsilon}_g\overline{u}_g + \frac{\gamma-2}{2}\overline{u}_g^2 & \gamma\overline{\varepsilon}_g + \frac{3-2\gamma}{2}\overline{u}_g^2 & \gamma\overline{u}_g \end{pmatrix} \tag{3.3}$$

is a Roe linearization of the jump conditions (2.9.i).

Next, matrix $\mathbf{A}_{22}^0$ *defined by*

$$\mathbf{A}_{22}^0(\mathbf{u}^L, \mathbf{u}^R) = \begin{pmatrix} 0 & 1 & 0\\ -\overline{u}_l^2 + X & 2\overline{u}_l^2 & 0\\ -\overline{e}_l\overline{u}_l + Y_1 & \overline{e}_l + Y_2 & \overline{u}_l \end{pmatrix}, \tag{3.4.i}$$

where

$$X = \begin{cases} \dfrac{\theta_0}{\rho_l}\dfrac{(1-\alpha^R)^\delta - (1-\alpha^L)^\delta}{\alpha^L - \alpha^R} & \text{if } \alpha^R \neq \alpha^L\\ \dfrac{\delta\theta_0}{\rho_l}(1-\alpha)^{\delta-1} & \text{if } \alpha^R = \alpha^L \end{cases} \tag{3.4.ii}$$

and

$$Y_1 = \begin{cases} \dfrac{\theta_0}{\rho_l}\dfrac{(1-\alpha^R)u_l^R + (1-\alpha^L)u_l^L}{2}\dfrac{(1-\alpha^R)^{\delta-1} - (1-\alpha^L)^{\delta-1}}{\alpha^L - \alpha^R} & \text{if } \alpha^R \neq \alpha^L\\ \dfrac{(\delta-1)\theta_0}{\rho_l}\dfrac{u_l^L + u_l^R}{2}(1-\alpha)^{\delta-2} & \text{if } \alpha^R = \alpha^L \end{cases} \tag{3.4.iii}$$

$$Y_2 = \frac{\theta_0}{2\rho_l}((1-\alpha^L)^{\delta-1} + (1-\alpha^R)^{\delta-1}) \tag{3.4.iv}$$

is a Roe linearization of the jump relations (2.9.ii).

Proof. Matrix (3.3) was introduced in [9] as a linearization of the jump conditions for the Euler system of gas dynamics:

$$\begin{pmatrix} [\alpha\rho_g u_g]\\ [\alpha\rho_g u_g^2 + \alpha p]\\ [\alpha\rho_g e_g u_g + \rho p u_g] \end{pmatrix} = \begin{pmatrix} 0 & 1 & 0\\ -\frac{3-\gamma}{2}\overline{u}_g^2 & (3-\gamma)\overline{u}_g & \gamma-1\\ -\gamma\overline{\varepsilon}_g\overline{u}_g + \frac{\gamma-2}{2}\overline{u}_g^3 & \gamma\overline{\varepsilon}_g + \frac{3-2\gamma}{2}\overline{u}_g^2 & \gamma\overline{u}_g \end{pmatrix} \cdot \begin{pmatrix} [\alpha\rho_g]\\ [\alpha\rho_g u_g]\\ [\alpha\rho_g e_g] \end{pmatrix}. \tag{3.5}$$

Next, the functions

$$((1-\alpha)^{1/2}, (1-\alpha)^{1/2}u_l, (1-\alpha)^{1/2}e_l) \to (1-\alpha, (1-\alpha)u_l, (1-\alpha)e_l)$$

and

$$((1-\alpha)^{1/2}, (1-\alpha)^{1/2}u_l, (1-\alpha)^{1/2}e_l) \to ((1-\alpha)u_l, (1-\alpha)u_l^2, (1-\alpha)e_l u_l)$$

are homogeneous with degree 2 so that

$$\begin{pmatrix} [1-\alpha]u_l \\ [(1-\alpha)u_l^2] \\ [(1-\alpha)e_l u_l] \end{pmatrix} = \begin{pmatrix} 0 & 1 & 0 \\ -\overline{u}_l^2 & 2\overline{u}_l & 0 \\ -\overline{e}_l\overline{u}_l & \overline{e}_l & \overline{u}_l \end{pmatrix} \cdot \begin{pmatrix} [1-\alpha] \\ [(1-\alpha)u_l] \\ [(1-\alpha)e_l] \end{pmatrix},$$

where the average quantities $\overline{1-\alpha}$, $\overline{u}_l$, and $\overline{e}_l$ are defined by (3.2.ii). Following [10] we write next

$$\begin{aligned} [\theta(\alpha)u_l] &= \left[\frac{\theta(\alpha)}{(1-\alpha)\rho_l}(1-\alpha)\rho_l u_l\right] \\ &= \frac{1}{2\rho_l}\left(\frac{\theta(\alpha^R)}{1-\alpha^R} + \frac{\theta(\alpha^L)}{1-\alpha^L}\right)[(1-\alpha)\rho_l u_l] \\ &\quad + \frac{(1-\alpha^R)u_l^R + (1-\alpha^L)u_l^L}{2}\left[\frac{\theta(\alpha)}{(1-\alpha)}\right]. \end{aligned}$$

This concludes the proof of Lemma 3.1. ∎

To obtain a linerarization of the jump relations (2.8) it remains to linearize the "perturbation" terms.

LEMMA 3.2. *Let* $\mathbf{u}^L$ *and* $\mathbf{u}^R$ *be two given states. Set*

$$\sigma = \begin{cases} -\dfrac{[\alpha\rho_g u_g + (1-\alpha)\rho_l u_l]}{[\alpha\rho_g + (1-\alpha)\rho_l]} & \text{if } [\alpha\rho_g + (1-\alpha)\rho_l] \neq 0 \\ 0 & \text{if } [\alpha\rho_g + (1-\alpha)\rho_l] = 0. \end{cases} \tag{3.6}$$

We define next the matrices

$$\mathbf{A}_{12}^1(\mathbf{u}^L, \mathbf{u}^R) = \begin{pmatrix} 0 & 0 & 0 \\ \alpha^L p^L Z & 0 & 0 \\ \sigma\alpha^L p^L Z & 0 & 0 \end{pmatrix} \tag{3.7.i}$$

$$\mathbf{A}_{21}^1(\mathbf{u}^L, \mathbf{u}^R) = \rho_l\left(\frac{1}{2\alpha^R} + \frac{1}{2\alpha^L} - 1\right) \begin{pmatrix} 0 & 0 & 0 \\ \dfrac{(\gamma-1)\overline{u}_g^2}{2} & (1-\gamma)\overline{u}_g & \gamma-1 \\ \sigma\dfrac{(\gamma-1)\overline{u}_g^2}{2} & (1-\gamma)\sigma\overline{u}_g & \sigma(\gamma-1) \end{pmatrix} \tag{3.7.ii}$$

$$\mathbf{A}_{22}^1(\mathbf{u}^L, \mathbf{u}^R) = \begin{pmatrix} 0 & 0 & 0 \\ -\alpha^L p^L Z + \dfrac{\alpha^L p^L + \alpha^R p^R}{2\alpha^L\alpha^R} & 0 & 0 \\ \sigma\alpha^L p^L Z + \sigma\dfrac{\alpha^L p^L + \alpha^R p^R}{2\alpha^L\alpha^R} & 0 & 0 \end{pmatrix}, \tag{3.7.iii}$$

where

$$Z = \begin{cases} \dfrac{[\log(\alpha)]}{[\alpha]} & \text{if } \alpha^L \neq \alpha^R \\ \dfrac{1}{\alpha^L} & \text{if } \alpha^L = \alpha^R. \end{cases} \tag{3.8}$$

The matrix

$$\begin{aligned} \tilde{\mathbf{A}}(\mathbf{u}^L, \mathbf{u}^R) &= \tilde{\mathbf{A}}^0(\mathbf{u}^L, \mathbf{u}^R) + \varepsilon\tilde{\mathbf{A}}^1(\mathbf{u}^L, \mathbf{u}^R) \\ &= \begin{pmatrix} \mathbf{A}_{11}^0 & \mathbf{0} \\ \mathbf{0} & \mathbf{A}_{22}^0 \end{pmatrix} + \varepsilon\begin{pmatrix} \mathbf{0} & \mathbf{A}_{12}^1 \\ \mathbf{A}_{21}^1 & \mathbf{A}_{22}^1 \end{pmatrix} \end{aligned} \tag{3.9}$$

is a Roe linearization of the approximate jump conditions (2.8); *conditions* (2.8) *and* (3.1) *are equivalent.*

Proof. According to Lemma 3.1, the perturbation terms that remain to be linearized are $\alpha^L p^L[\log(\alpha)]$, $[(1-\alpha)p]$, and the same terms multiplied by the number σ. We first write

$$\alpha^L p^L[\log(\alpha)] = -\frac{\alpha^L p^L}{\rho_l}\frac{[\log(\alpha)]}{[\alpha]}([(1-\alpha)\rho_l]$$

and we deduce matrix $\mathbf{A}_{12}^1$. Next,

$$\begin{aligned} [p(1-\alpha)] &= \left[\frac{\alpha p}{\alpha}\right] - [\alpha p] \\ &= \left(\frac{1}{2\alpha^R} + \frac{1}{2\alpha^L} - 1\right)[\alpha p] - \frac{\alpha^L p^L + \alpha^R p^R}{2\rho_l\alpha^L\alpha^R}[(1-\alpha)\rho_l]. \end{aligned}$$

The jump $[\alpha p]$ is linearized following (3.5), which yields matrix $\mathbf{A}_{21}^1$ while the other term is included in matrix $\mathbf{A}_{22}^1$. ∎

Remark 3.1. Note that when the numbers $1-\alpha^L$ and $1-\alpha^R$ are of order ε, the matrix $\mathbf{A}^1$ is of order zero so that $\tilde{\mathbf{A}}$ is a perturbation of order 1 in ε of matrix $\tilde{\mathbf{A}}^0$.

Using the linearization (3.9) that we introduced, the numerical scheme (written in nonconservation form) reads

$$\mathbf{u}_j^{n+1} = \mathbf{u}_j^n - \frac{\Delta t}{\Delta x}((\tilde{\mathbf{A}}(\mathbf{u}_j^n, \mathbf{u}_{j+1}^n))^-(\mathbf{u}_{j+1}^n - \mathbf{u}_j^n) + (\tilde{\mathbf{A}}(\mathbf{u}_{j-1}^n, \mathbf{u}_j^n))^+(\mathbf{u}_j^n - \mathbf{u}_{j-1}^n)), \tag{3.10}$$

where $\mathbf{u}_j^n$ stands for an approximation of the solution $\mathbf{u}$ of

where $\phi(\mathbf{u}, \mathbf{v})$ is the numerical flux of Roe scheme:

$$\begin{aligned}\phi(\mathbf{u}, \mathbf{v}) &= \mathbf{h}(\mathbf{u}) + (\mathbf{C}(\mathbf{u}, \mathbf{v}))^-(\mathbf{v} - \mathbf{u}) \\ &= \mathbf{h}(\mathbf{v}) - (\mathbf{C}(\mathbf{u}, \mathbf{v}))^+(\mathbf{v} - \mathbf{u}) \\ &= \frac{\mathbf{h}(\mathbf{u}) + \mathbf{h}(\mathbf{v})}{2} - \frac{|\mathbf{C}(\mathbf{u}, \mathbf{v})|}{2}(\mathbf{v} - \mathbf{u}).\end{aligned} \tag{3.16}$$

We prove the following.

LEMMA 3.3. *The scheme* (3.15) *takes the nonconservation form:*

$$\mathbf{r}_4^0 = \begin{pmatrix} 0 \\ 0 \\ 0 \\ 1 \\ \bar{u}_l - \bar{c}_l \\ \bar{e}_l - \dfrac{Y_1}{\bar{c}_l} - Y_2\dfrac{\bar{u}_l - \bar{c}_l}{\bar{c}_l} \end{pmatrix},$$

$$\mathbf{r}_5^0 = \begin{pmatrix} 0 \\ 0 \\ 0 \\ 1 \\ \bar{u}_l + \bar{c}_l \\ \bar{e}_l + \dfrac{Y_1}{\bar{c}_l} + Y_2\dfrac{\bar{u}_l + \bar{c}_l}{\bar{c}_l} \end{pmatrix}, \quad \mathbf{r}_6^0 = \begin{pmatrix} 0 \\ 0 \\ 0 \\ 0 \\ 0 \\ 1 \end{pmatrix}, \tag{4.5}$$

where Y_1 *and* Y_2 *are defined by* (3.4.iii) *and* (3.4.iv). *The corresponding left eigenvectors are*

$$\mathbf{l}_4^0 = \begin{pmatrix} 0 \\ 0 \\ 0 \\ \dfrac{\bar{u}_l + \bar{c}_l}{2\bar{c}_l} \\ -\dfrac{1}{2\bar{c}_l} \\ 0 \end{pmatrix}, \quad \mathbf{l}_5^0 = \begin{pmatrix} 0 \\ 0 \\ 0 \\ \dfrac{\bar{c}_l - \bar{u}_l}{2\bar{c}_l} \\ \dfrac{1}{2\bar{c}_l} \\ 0 \end{pmatrix}, \tag{4.6}$$

$$\begin{pmatrix} 0 \\ 0 \\ 0 \end{pmatrix}$$

ε the following approximate eigenvalues and eigenvectors for matrix $\tilde{\mathbf{A}}^1(\mathbf{u}^L, \mathbf{u}^R)$:

$$\lambda_k = \lambda_k^0 + \varepsilon\lambda_k^1 + O(\varepsilon^2) \tag{4.7.i}$$

where

$$\lambda_k^1 = (\mathbf{l}_k^0, \tilde{\mathbf{A}}^1\mathbf{r}_k^0) \tag{4.7.ii}$$

and

$$\mathbf{r}_k = \mathbf{r}_k^0 + \varepsilon\mathbf{r}_k^1 + O(\varepsilon^2), \tag{4.8.i}$$

where

$$\mathbf{r}_k^1 = \sum_{\substack{m=1 \\ m\neq k}}^{6} \frac{-1}{\lambda_m^0 - \lambda_k^0}(\mathbf{l}_m^0, \tilde{\mathbf{A}}^1\mathbf{r}_k^0)\mathbf{r}_m^0. \tag{4.8.ii}$$

Proof. Assume that matrix $\tilde{\mathbf{A}}^0(\mathbf{u}^L, \mathbf{u}^R)$ has six distinct eigenvalues. We look for some approximate eigenvalues and eigenvectors of matrix $\tilde{\mathbf{A}}(\mathbf{u}^L, \mathbf{u}^R)$ in the form

$$\lambda_k(\mathbf{u}^L, \mathbf{u}^R) = \sum_{p=0}^{+\infty} \varepsilon^p\lambda_k^p(\mathbf{u}^L, \mathbf{u}^R), \quad \mathbf{r}_k(\mathbf{u}^L, \mathbf{u}^R) = \sum_{p=0}^{+\infty} \varepsilon^p\mathbf{r}_k^p(\mathbf{u}^L, \mathbf{u}^R).$$

Vector $\mathbf{r}_k$ is an eigenvector of matrix $\tilde{\mathbf{A}} = \tilde{\mathbf{A}}^0 + \varepsilon\tilde{\mathbf{A}}^1$ associated with the eigenvalue λ_k if

$$(\tilde{\mathbf{A}}^0 + \varepsilon\tilde{\mathbf{A}}^1)\sum_{p=0}^{+\infty} \varepsilon^p\mathbf{r}_k^p = \left(\sum_{p=0}^{+\infty} \varepsilon^p\lambda_k^p\right)\left(\sum_{p=0}^{+\infty} \varepsilon^p\mathbf{r}_k^p\right). \tag{4.9}$$

At zeroth order in ε, we get

$$\tilde{\mathbf{A}}^0\mathbf{r}_k^0 = \lambda_k^0\mathbf{r}_k^0.$$

Hence, at zeroth order in ε, the eigenvector $\mathbf{r}_k$ and the eigenvalue λ_k are given by expressions (4.3)–(4.5). Next at first order,

4. IMPLEMENTATION OF THE NUMERICAL SCHEME

We describe below an efficient implementation of the numerical schemes (3.10) and (3.19). An implementation of these two schemes requires *a priori* to know the eigenvalues and eigenvectors of the linearization matrix (3.9) for any two states $\mathbf{u}^L$ and $\mathbf{u}^R$. Various linear algebra packages offer a numerical solution to this problem. This leads, however, to a very expensive computer code.

Recall, however, that when the volume fraction of the liquid phase is of order ε, the linearization matrix (3.9) is a perturbation of order ε of matrix $\tilde{\mathbf{A}}^0(\mathbf{u}^L, \mathbf{u}^R)$ whose eigenvalues and eigenvectors are explicitly known. A perturbation method enables us to obtain approximate eigenvalues and eigenvectors of matrix $\tilde{\mathbf{A}}(\mathbf{u}^L, \mathbf{u}^R)$. We give next a simple algorithm to decompose any vector in $\mathbb{R}^6$ on the obtained approximate eigenbasis of matrix $\tilde{\mathbf{A}}(\mathbf{u}^L, \mathbf{u}^R)$.

Matrix $\tilde{\mathbf{A}}^0(\mathbf{u}^L, \mathbf{u}^R)$ has a simple structure and we can compute its eigenvalues and left and right eigenvectors.

LEMMA 4.1. *Matrix* $\tilde{\mathbf{A}}^0(\mathbf{u}^L, \mathbf{u}^R)$ *has the eigenvalues*

$$\begin{aligned} \lambda_1^0 &= \bar{u}_g - \bar{c}_g \\ \lambda_2^0 &= \bar{u}_g + \bar{c}_g \\ \lambda_3^0 &= \bar{u}_g, \end{aligned} \tag{4.1}$$

where the gas sound speed $\bar{c}_g$ *is*

$$\bar{c}_g = \sqrt{\gamma(\gamma-1)\bar{\varepsilon}_g},$$

and

$$\begin{aligned} \lambda_4^0 &= \bar{u}_l - \bar{c}_l \\ \lambda_5^0 &= \bar{u}_l + \bar{c}_l \\ \lambda_6^0 &= \bar{u}_l, \end{aligned} \tag{4.2}$$

where the speed $\bar{c}_l$ *is*

$$\bar{c}_l = \begin{cases} \sqrt{\dfrac{\theta_0}{\rho_l}\dfrac{(1-\alpha^R)^\delta - (1-\alpha^L)^\delta}{\alpha^R - \alpha^L}} & \text{if } \alpha^R \neq \alpha^L \\ \sqrt{\dfrac{\delta\theta_0}{\rho_l}(1-\alpha^R)^{\delta-1}} & \text{if } \alpha^R = \alpha^L. \end{cases}$$

The right eigenvectors associated with eigenvalues λ_i, $i = 1, \ldots, 3$, *are respectively*

$$\mathbf{r}_1^0 = \begin{pmatrix} 1 \\ \bar{u}_g - \bar{c}_g \\ \dfrac{\bar{u}_g^2}{2} - \bar{u}_g\bar{c}_g + \dfrac{\bar{c}_g^2}{\gamma-1} \\ 0 \\ 0 \\ 0 \end{pmatrix}, \quad \mathbf{r}_2^0 = \begin{pmatrix} 1 \\ \bar{u}_g + \bar{c}_g \\ \dfrac{\bar{u}_g^2}{2} + \bar{u}_g\bar{c}_g + \dfrac{\bar{c}_g^2}{\gamma-1} \\ 0 \\ 0 \\ 0 \end{pmatrix}, \quad \mathbf{r}_3^0 = \begin{pmatrix} 1 \\ \bar{u}_g \\ \dfrac{\bar{u}_g^2}{2} \\ 0 \\ 0 \\ 0 \end{pmatrix}. \tag{4.3}$$

The corresponding left eigenvectors are

$$\mathbf{l}_1^0 = \begin{pmatrix} \dfrac{(\gamma-1)\bar{u}_g^2}{4\bar{c}_g^2} + \dfrac{\bar{u}_g}{2\bar{c}_g} \\ -\dfrac{1}{2\bar{c}_g} - \dfrac{(\gamma-1)\bar{u}_g}{2\bar{c}_g^2} \\ \dfrac{(\gamma-1)}{\bar{c}_g^2} \\ 0 \\ 0 \\ 0 \end{pmatrix}, \quad \mathbf{l}_2^0 = \begin{pmatrix} \dfrac{(\gamma-1)\bar{u}_g^2}{4\bar{c}_g^2} - \dfrac{\bar{u}_g}{2\bar{c}_g} \\ \dfrac{1}{2\bar{c}_g} - \dfrac{(\gamma-1)\bar{u}_g}{2\bar{c}_g^2} \\ \dfrac{(\gamma-1)}{\bar{c}_g^2} \\ 0 \\ 0 \\ 0 \end{pmatrix}, \tag{4.4}$$

$$\mathbf{l}_3^0 = \begin{pmatrix} 1 - \dfrac{\bar{u}_g^2}{2(\gamma-1)\bar{c}_g^2} \\ \dfrac{(\gamma-1)\bar{u}_g}{\bar{c}_g^2} \\ \dfrac{(1-\gamma)}{\bar{c}_g^2} \\ 0 \\ 0 \\ 0 \end{pmatrix}.$$

The right eigenvectors associated with eigenvalues λ_i, $i = 4, \ldots, 6$, *are respectively*

$$\mathbf{r}_4^0 = \begin{pmatrix} 0 \\ 0 \\ 0 \\ 1 \\ \overline{u}_l - \overline{c}_l \\ \overline{e}_l - \dfrac{Y_1}{\overline{c}_l} - Y_2 \dfrac{\overline{u}_l - \overline{c}_l}{\overline{c}_l} \end{pmatrix},$$

$$\mathbf{r}_5^0 = \begin{pmatrix} 0 \\ 0 \\ 0 \\ 1 \\ \overline{u}_l + \overline{c}_l \\ \overline{e}_l + \dfrac{Y_1}{\overline{c}_l} + Y_2 \dfrac{\overline{u}_l + \overline{c}_l}{\overline{c}_l} \end{pmatrix}, \quad \mathbf{r}_6^0 = \begin{pmatrix} 0 \\ 0 \\ 0 \\ 0 \\ 0 \\ 1 \end{pmatrix}, \tag{4.5}$$

where Y_1 and Y_2 are defined by (3.4.iii) *and* (3.4.iv). *The corresponding left eigenvectors are*

$$\mathbf{l}_4^0 = \begin{pmatrix} 0 \\ 0 \\ 0 \\ \dfrac{\overline{u}_l + \overline{c}_l}{2\overline{c}_l} \\ -\dfrac{1}{2\overline{c}_l} \\ 0 \end{pmatrix}, \quad \mathbf{l}_5^0 = \begin{pmatrix} 0 \\ 0 \\ 0 \\ \dfrac{\overline{c}_l - \overline{u}_l}{2\overline{c}_l} \\ \dfrac{1}{2\overline{c}_l} \\ 0 \end{pmatrix},$$

$$\mathbf{l}_6^0 = \begin{pmatrix} 0 \\ 0 \\ 0 \\ -\overline{e}_l + \dfrac{\overline{u}_l}{\overline{c}_l^2} Y_1 + Y_2 \dfrac{\overline{u}_l^2 - \overline{c}_l^2}{\overline{c}_l^2} \\ -\dfrac{Y_1}{\overline{c}_l^2} - Y_2 \dfrac{\overline{u}_l}{\overline{c}_l^2} \\ 1 \end{pmatrix}. \tag{4.6}$$

Recalling that matrix $\tilde{\mathbf{A}}^1$ is a perturbation of order ε of matrix $\tilde{\mathbf{A}}^0$, we can obtain next approximate eigenvalues and eigenvectors of matrix $\tilde{\mathbf{A}}^1(\mathbf{u}^L, \mathbf{u}^R)$ as follows.

PROPOSITION 4.2. *Let be given two states $\mathbf{u}^L$ and $\mathbf{u}^R$. Assume that matrix $\tilde{\mathbf{A}}^0(\mathbf{u}^L, \mathbf{u}^R)$ has six distinct eigenvalues λ_i^0, $1 \leq i \leq 6$. Then for ε small enough, we obtain at the first order in ε the following approximate eigenvalues and eigenvectors for matrix $\tilde{\mathbf{A}}^1(\mathbf{u}^L, \mathbf{u}^R)$:*

$$\lambda_k = \lambda_k^0 + \varepsilon \lambda_k^1 + O(\varepsilon^2) \tag{4.7.i}$$

where

$$\lambda_k^1 = (\mathbf{l}_k^0, \tilde{\mathbf{A}}^1 \mathbf{r}_k^0) \tag{4.7.ii}$$

and

$$\mathbf{r}_k = \mathbf{r}_k^0 + \varepsilon \mathbf{r}_k^1 + O(\varepsilon^2), \tag{4.8.i}$$

where

$$\mathbf{r}_k^1 = \sum_{\substack{m=1 \\ m \neq k}}^{6} \frac{-1}{\lambda_m^0 - \lambda_k^0} (\mathbf{l}_m^0, \tilde{\mathbf{A}}^1 \mathbf{r}_k^0) \mathbf{r}_m^0. \tag{4.8.ii}$$

Proof. Assume that matrix $\tilde{\mathbf{A}}^0(\mathbf{u}^L, \mathbf{u}^R)$ has six distinct eigenvalues. We look for some approximate eigenvalues and eigenvectors of matrix $\tilde{\mathbf{A}}(\mathbf{u}^L, \mathbf{u}^R)$ in the form

$$\lambda_k(\mathbf{u}^L, \mathbf{u}^R) = \sum_{p=0}^{+\infty} \varepsilon^p \lambda_k^p(\mathbf{u}^L, \mathbf{u}^R), \quad \mathbf{r}_k(\mathbf{u}^L, \mathbf{u}^R) = \sum_{p=0}^{+\infty} \varepsilon^p \mathbf{r}_k^p(\mathbf{u}^L, \mathbf{u}^R).$$

Vector $\mathbf{r}_k$ is an eigenvector of matrix $\tilde{\mathbf{A}} = \tilde{\mathbf{A}}^0 + \varepsilon \tilde{\mathbf{A}}^1$ associated with the eigenvalue λ_k if

$$(\tilde{\mathbf{A}}^0 + \varepsilon \tilde{\mathbf{A}}^1) \sum_{p=0}^{+\infty} \varepsilon^p \mathbf{r}_k^p = \left(\sum_{p=0}^{+\infty} \varepsilon^p \lambda_k^p \right) \left(\sum_{p=0}^{+\infty} \varepsilon^p \mathbf{r}_k^p \right). \tag{4.9}$$

At zeroth order in ε, we get

$$\tilde{\mathbf{A}}^0 \mathbf{r}_k^0 = \lambda_k^0 \mathbf{r}_k^0.$$

Hence, at zeroth order in ε, the eigenvector $\mathbf{r}_k$ and the eigenvalue λ_k are given by expressions (4.3)–(4.5). Next at first order, (4.9) gives

$$(\tilde{\mathbf{A}}^0 - \lambda_k^0 \mathbf{1}) \mathbf{r}_k^1 = -(\tilde{\mathbf{A}}^1 - \lambda_k^1 \mathbf{1}) \mathbf{r}_k^0. \tag{4.10}$$

Multiplying this latter identity on the left by the left eigenvector $\mathbf{l}_k^0$ of matrix $\tilde{\mathbf{A}}^0$, we obtain that the number λ_k^1 is given by the scalar product:

$$\lambda_k^1 = (\mathbf{l}_k^0, \tilde{\mathbf{A}}^1 \mathbf{r}_k^0).$$

Next, the vector $\mathbf{r}_k^1$ solution of (4.10) is given by

$$\mathbf{r}_k^1 = \sum_{\substack{m=1 \\ m \neq k}}^{6} \frac{-1}{\lambda_m^0 - \lambda_k^0} (\mathbf{l}_m^0, \tilde{\mathbf{A}}^1 \mathbf{r}_k^0) \mathbf{r}_m^0. \quad \blacksquare$$

The computation of the approximate eigenvalues and eigenvectors relies on the assumption that matrix $\tilde{\mathbf{A}}^0$ has six distinct eigenvalues. Indeed formula (4.8) is not defined when $\tilde{\mathbf{A}}^0$ has a double eigenvalue. According to Lemma 4.1, matrix $\tilde{\mathbf{A}}^0$ has a double eigenvalue when one of the following conditions holds:

$$\overline{u}_g \pm \overline{c}_g = \overline{u}_l, \quad \overline{u}_g \pm \overline{c}_g = \overline{u}_l \pm \overline{c}_l, \quad \overline{u}_g = \overline{u}_l \pm \overline{c}_l.$$

Due to the drag force, the relative velocities of the gas and dispersed phases are close together. On the other hand, note that the number $\overline{c}_l$ is rather small. Hence, the only physical case to retain is

$$\overline{u}_g = \overline{u}_l \pm \overline{c}_l.$$

In that case the computer code fails. Note, however, that system (1.3) is hyperbolic over the whole set Ω_g^M, *i.e.*, that the difficulty arises from the numerical treatment.

To overcome this difficulty, when computing an approximate eigenvalue λ_k of matrix $\tilde{\mathbf{A}}(\mathbf{u}^L, \mathbf{u}^R)$, we can replace the number σ that appears in matrix $\tilde{\mathbf{A}}^1$ by the eigenvalue λ_k^0 of matrix $\tilde{\mathbf{A}}^0$. Indeed the Roe linearization $\tilde{\mathbf{A}}(\mathbf{u}^L, \mathbf{u}^R)$ is designed so that when $\mathbf{u}^L$ and $\mathbf{u}^R$ are connected by a shock wave with speed σ, the vector $\mathbf{u}^R - \mathbf{u}^L$ is an eigenvector of matrix $\tilde{\mathbf{A}}$ associated with the eigenvalue σ. In this case, the number σ is precisely the number that appears in matrix $\tilde{\mathbf{A}}^1$. Expecting that this eigenvalue σ of matrix $\tilde{\mathbf{A}}$ is a perturbation of order ε of some eigenvalue λ_k^0 of $\tilde{\mathbf{A}}^0$, we can replace σ in $\tilde{\mathbf{A}}^1$ by λ_k^0. Matrix $\tilde{\mathbf{A}}$ is then modified at second order in ε and we keep first-order accuracy in the computations. With this approximation, formula (4.8) is no longer singular. Indeed we have the following.

PROPOSITION 4.3. *For $i = 3$ or $i = 6$, eigenvector $\mathbf{r}_i^0$ is an eigenvector of matrix $\tilde{\mathbf{A}}$, where number σ in $\tilde{\mathbf{A}}^1$ has been replaced by λ_i^0. Next for $i = 4$, 5, the computation of the approximate eigenvector $\mathbf{r}_i$ with formula* (4.8) *is nonsingular when the number σ in matrix $\tilde{\mathbf{A}}^1$ is replaced by λ_i^0.*

Proof. First, when $\sigma = \overline{u}_g$, we have that

$$\mathbf{A}_{2l}^1 \begin{pmatrix} 1 \\ \overline{u}_g \\ \dfrac{\overline{u}_g^2}{2} \end{pmatrix} = \mathbf{0}$$

so that $\mathbf{A}^1 \mathbf{r}_3^0 = 0$: vector $\mathbf{r}_3^0$ is an eigenvector of matrix $\mathbf{A}$, provided that $\sigma = \overline{u}_g$.

For any value of σ, we have $\tilde{\mathbf{A}}^1 \mathbf{r}_6^0 = \mathbf{0}$ so that $\mathbf{r}_6^0$ is always an eigenvector of matrix $\tilde{\mathbf{A}}$.

Choose next $i = 4$ or $i = 5$. The only *a priori* singular term in formula (4.8) is $1/(\lambda_m^0 - \lambda_i^0)$ for $m = 3$ and $\lambda_m^0 = \overline{u}_g = \lambda_i^0$. But when σ in matrix $\tilde{\mathbf{A}}^1$ equals $\overline{u}_g$, we have

$$\left(1 - \frac{\overline{u}_g^2}{2(\gamma - 1)\overline{c}_g^2}, \frac{(\gamma - 1)\overline{u}_g}{\overline{c}_g^2}, \frac{(1 - \gamma)}{\overline{c}_g^2}\right) \cdot \mathbf{A}_{l2}^1 = 0.$$

More generally, for $\sigma = \lambda_i^0$ close from $\overline{u}_g$, we compute

$$\left(1 - \frac{\overline{u}_g^2}{2(\gamma - 1)\overline{c}_g^2}, \frac{(\gamma - 1)\overline{u}_g}{\overline{c}_g^2}, \frac{(1 - \gamma)}{\overline{c}_g^2}\right) \cdot \mathbf{A}_{l2}^1 = (\overline{u}_g - \sigma)\left(\frac{(\gamma - 1)\alpha^L p^L}{\overline{c}_g^2}, 0, 0\right)$$

so that formula (4.8) is nonsingular when σ is replaced by λ_i^0. ∎

Remark 4.1. Replacing σ by λ_k^0 in matrix $\tilde{\mathbf{A}}^1$ is only valid (up to second order in ε) for exact shock data but seems inappropriate for numerically diffused profiles. This problem is a general problem for Roe-type methods which are built to solve only exact shock data. However, Roe-type methods give very good results and it seems that any two intermediate shock points in a numerically diffused profile given by a Roe-type method can approximately be connected by a shock wave with the velocity of the exact shock wave. This would (as well as the numerical results below do) justify our approximation.

It finally remains us to decompose any vector in $\mathbb{R}^6$ on the approximate eigenbasis $\mathbf{r}_k$ of matrix $\tilde{\mathbf{A}}(\mathbf{u}^L, \mathbf{u}^R)$ computed in Proposition 4.2. This is done easily thanks to the following.

PROPOSITION 4.4. *Let $\mathbf{y}$ be a given vector in $\mathbb{R}^6$. Then*

$$\mathbf{y} = \sum_{i=1}^{6} \left[(\mathbf{l}_i^0, \mathbf{y}) + \varepsilon \sum_{i=1}^{6} \left(\mathbf{l}_i^0, \sum_{j=1}^{6} y_j^0 \mathbf{r}_j^1 \right) \right] (\mathbf{r}_i^0 + \varepsilon \mathbf{r}_i^1) + O(\varepsilon^2). \tag{4.11}$$

Proof. We decompose a given vector $\mathbf{y}$ in $\mathbb{R}^6$ as

$$\mathbf{y} = \sum_{p=0}^{+\infty} \varepsilon^p \left(\sum_{i=1}^{6} y_i^p (\mathbf{r}_i^0 + \varepsilon \mathbf{r}_i^1) \right). \tag{4.12}$$

Expression (4.12) at zeroth order in ε reads

$$\sum_{i=1}^{6} y_i^0 \mathbf{r}_i^0 = \mathbf{y},$$

so that $y_i^0 = (\mathbf{l}_i^0, \mathbf{y})$. Next, at first-order it reads

$$\sum_{i=1}^{6} y_i^0 \mathbf{r}_i^1 + y_i^1 \mathbf{r}_i^0 = \mathbf{0}.$$

This yields

$$y_i^j = \left(\mathbf{l}_i^0, \sum_{j=1}^{6} y_i^0 \mathbf{r}_j^j\right).$$

This gives formula (4.11). ∎

Finally the approximations we considered allow us to compute in a simple manner and at a low cost the vector $|\tilde{\mathbf{A}}(\mathbf{u}^L, \mathbf{u}^R)|\mathbf{y}$ for $\mathbf{u}^L, \mathbf{u}^R \in \Omega$ and $\mathbf{y} \in \mathbb{R}^6$ given: if $\mathbf{r}_1, \ldots, \mathbf{r}_6$ denote the approximate eigenvectors defined by (4.8), we write

$$|\tilde{\mathbf{A}}(\mathbf{u}^L, \mathbf{u}^R)|\mathbf{y} \simeq \sum_{i=1}^{6} y_i |\lambda_i| \mathbf{r}_i, \tag{4.13}$$

where the numbers y_i, λ_i and the vectors $\mathbf{r}_i$ are respectively defined by (4.11), (4.7), and (4.8). This gives a simple, efficient, and low cost second order numerical scheme for system (1.3).

We compute the solution given by our numerical scheme when the initial data is a discontinuous profile that connects the left and right states given either in Table I or II of Section 2. Recall that the left and right states given in both tables satisfy the approximate jump conditions (2.8) for some known shock speed σ. We let the computer code run for some physical time T_0. The expected solution is the initial profile moved from the initial position by the distance σT_0, where σ is the speed of the shock wave. We plot on the same figure the computed solution and the expected solution. We can thus compare the profile and the speed of the computed wave with the expected profile and speed of the shock wave. We performed this test for the two shock wave examples given in section 2. Recall that these shock waves are representative of the different shock solutions of (1.3), since the first one mainly affects the gas quantities while the second one affects the liquid phase quantities. Figure 1 gives the results obtained for the first shock wave. The physical time of computation is $T_0 = 5 \times 10^{-3}$ s. The computed solution for this first example is excellent regarding both the shape of the profiles of the quantities associated with the gas phase and the speed of the wave. However, the left gas volume fraction and liquid phase velocities are close but distinct from the expected quantities; some waves have gone out of the computational domain and given a wrong left state. It is, however, to be noted that this error is very small and stationary in time. Furthermore the velocity of the computed gas volume fraction and the liquid phase profiles are correct.

Next, Fig. 2 shows the results obtained for the second shock wave of Section 3. The physical time of the simulation is $T_0 = 2.10^{-2}$ s. The connected states and the velocity of the shock wave are correct; only the gas temperature profile shows a small deviation from the expected profile. But here, again, the velocity of the computed wave is correct. We note the presence of a second wave apart from the main shock wave. This wave arises in the computed solution because of the different approximations we introduced in Section 3. The profiles are here more diffuse than the profiles of Fig. 1; this is a general pattern of Roe-type methods which give sharper shock profiles for stronger shocks.

We compare next our scheme with two different methods described respectively in [5, 6]. These two methods have in common to simplify the treatment of the coupling between the two phases, either by decomposing the initial nonconservative system into two conservative decoupled systems plus nonconservative coupling terms seen as production terms as in [5] or by retaining a zeroth-order expansion in $1 - \alpha$ of system (1.3) as in [6].

The method developed in [5] consists in writing system (1.3) in the form

$$\begin{aligned}
&\partial_t(\alpha\rho_g) + \partial_x(\alpha\rho_g u_g) = 0\\
&\partial_t(\alpha\rho_g u_g) + \partial_x(\alpha\rho_g u_g^2) + \partial_x(\alpha p) = p\partial_x\alpha\\
&\partial_t(\alpha\rho_g e_g) + \partial_x(\alpha\rho_g e_g u_g) + \partial_x(\alpha p u_g) = -p\partial_x((1-\alpha)u_i)
\end{aligned} \tag{4.14i}$$

$$\begin{aligned}
&\partial_t((1-\alpha)\rho_i) + \partial_x((1-\alpha)\rho_i u_i) = 0\\
&\partial_t((1-\alpha)\rho_i u_i) + \partial_x((1-\alpha)\rho_i u_i^2) + \partial_x\theta = -(1-\alpha)\partial_x p\\
&\partial_t((1-\alpha)\rho_i e_i) + \partial_x((1-\alpha)\rho_i e_i u_i) + \partial_x(\theta u_i) = -(1-\alpha)u_i\partial_x p.
\end{aligned} \tag{4.14ii}$$

Note that the two conservative systems in the left-hand side of (4.14) are decoupled. The coupling between the two phases only appears in the production terms. In [5], Toro proposes to solve this system using a time splitting: for each time step, he first solves the two conservative decoupled systems in the left-hand side of (4.14) and, second, he integrates explicitly the production terms which are estimated using a second-order centered difference scheme. This method leads to a robust solver.

We give in Fig. 3 the profiles obtained with this method for initial data from Table I in Section 2. The results are excellent. The speed of the shock wave is very accurately computed and the computed wave connects the correct states. We give next in Fig. 4 the results obtained with Toro's method at first order for the second shock wave of Section 2. The computed profiles are very diffusive but connect the right states (apart from the gas temperature). The liquid phase velocity profile is, however, composed of several waves, instead of a single one. We give next in Figs. 5 and 6 the results obtained with a Toro's method at second order for two physical times: $T_0 = 10^{-2}$ s for Fig. 5 and $T_0 = 3.10^{-2}$ s for Fig. 6. The profiles are sharper. However, we note the presence in the computed solution of a perturbation that grows in time. In Fig. 6, the computed solution is far away from the expected one.

In our opinion, the main drawbacks of this numerical scheme is that the obtained profile depends upon the order of the method; recall that any Godunov-type solver generates some numerical viscosity whose amount depends on the order of

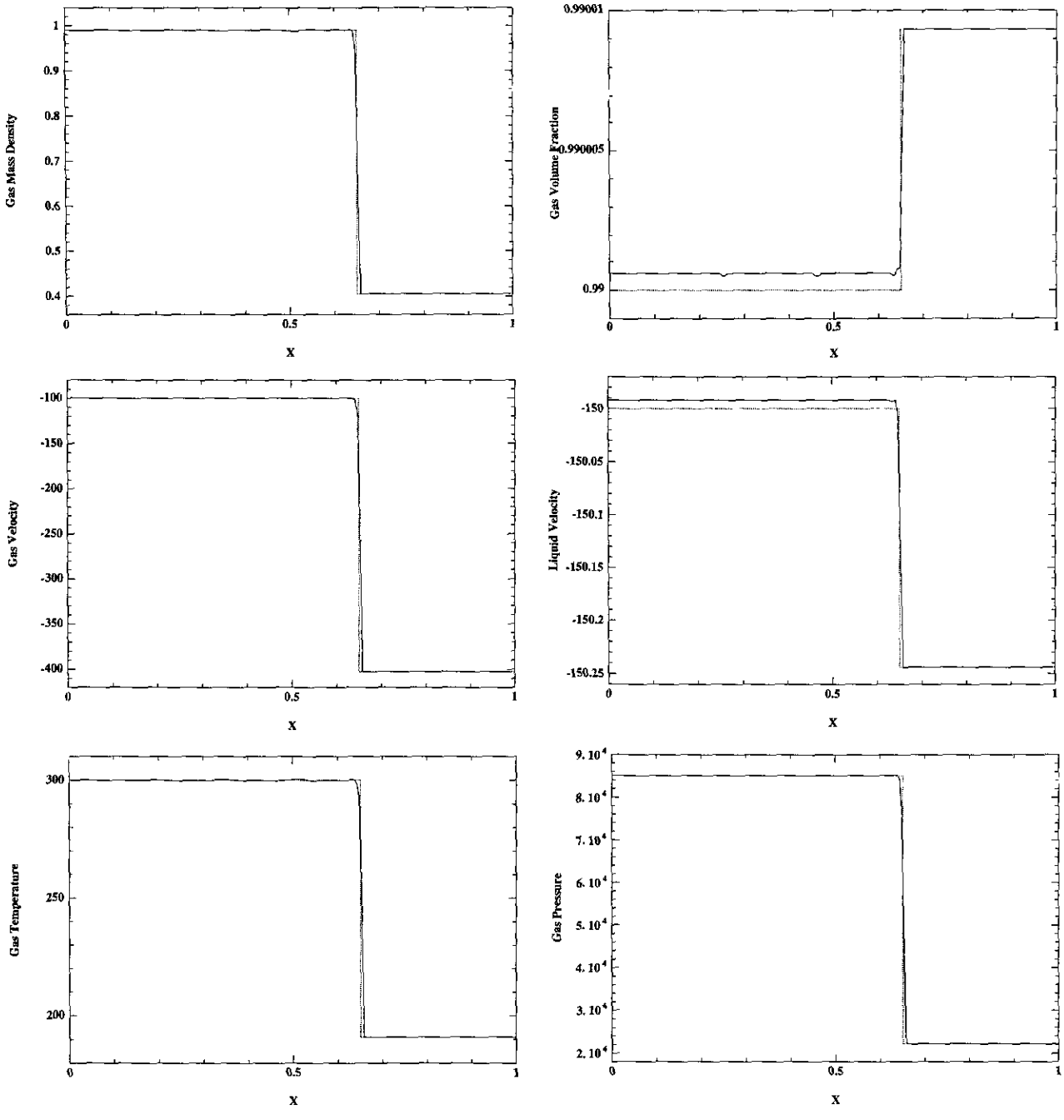

FIG. 1. Shock wave 1. Method 1 at second order, $T_0 = 5 \times 10^{-3}$ s.

the method. Hence, Toro's numerical scheme computes some solution of system (1.3) in which some diffusion tensor, introduced by the numerical method, has been added. But system (1.3) is in nonconservation form and as noted in Section 1, the states that can be connected by a traveling wave solution of (1.3) in which a numerical viscosity tensor has been added depend on this latter tensor. Unlike the method proposed in this paper, Toro's method is not compatible with the physical diffusion tensor so that, when using Toro's method, a different rarefaction and shock wave pattern is selected. Diffusion plays an important role in the definition of shock wave 2 in Section 2; the wave pattern selected by Toro's method is indeed distinct from the expected single shock wave and depends on the order of the method.

We introduce in [6] a simplification of system (1.3) based on the analysis described in [8]. Recall that for two phase fluid flows of interest, the volume fraction $1 - \alpha$ of the liquid phase is of order ρ_g/ρ_l and is small in comparison with 1. In Section 3, we took advantage of this fact to write a first-order expansion (2.8) of the jump conditions (1.6). In [6], we simply take this

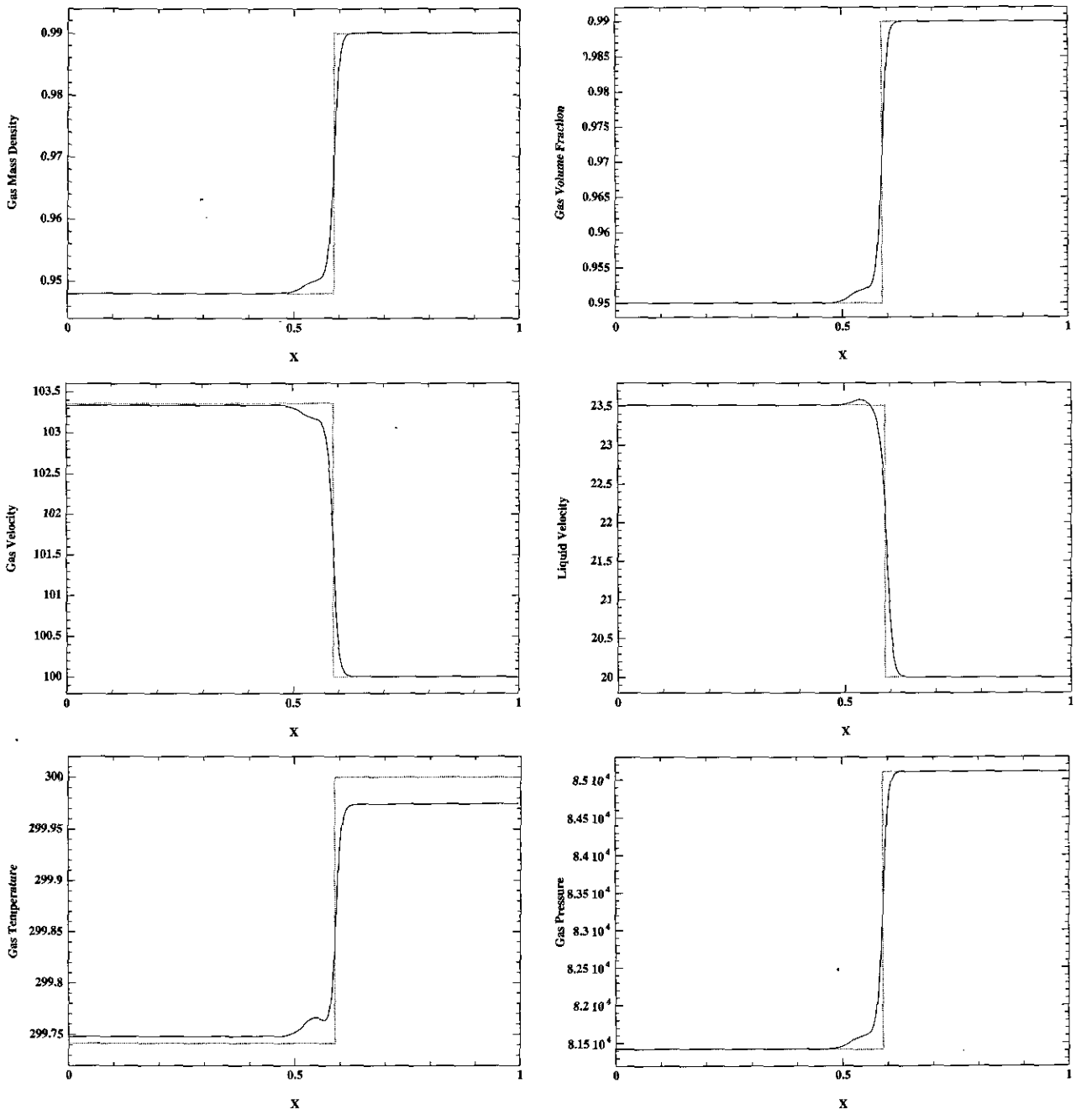

FIG. 2. Shock wave 2. Method 1 at second order, $T_0 = 2 \times 10^{-2}$ s.

expansion at zeroth-order in $1 - \alpha$, which means that we solve the following decoupled two systems:

$$\begin{aligned}
\partial_t(\alpha\rho_g) + \partial_x(\alpha\rho_g u_g) &= 0\\
\partial_t(\alpha\rho_g u_g) + \partial_x(\alpha\rho_g u_g^2) + \partial_x(\alpha p) &= 0\\
\partial_t(\alpha\rho_g e_g) + \partial_x(\alpha\rho_g e_g u_g) + \partial_x(\alpha p u_g) &= 0 \qquad (4.15.\text{i})
\end{aligned}$$

$$\begin{aligned}
\partial_t((1-\alpha)\rho_l) + \partial_x((1-\alpha)\rho_l u_l) &= 0\\
\partial_t((1-\alpha)\rho_l u_l) + \partial_x((1-\alpha)\rho_l u_l^2 + \theta_0(1-\alpha)^\delta) &= 0\\
\partial_t((1-\alpha)\rho_l e_l) + \partial_x((1-\alpha)\rho_l e_l u_l) + \partial_x(\theta_0(1-\alpha)^\delta u_l) &= 0. \qquad (4.15.\text{ii})
\end{aligned}$$

The first system is simply the Euler system of gas dynamics, where the gas mass density ρ_g has been replaced by the quantity

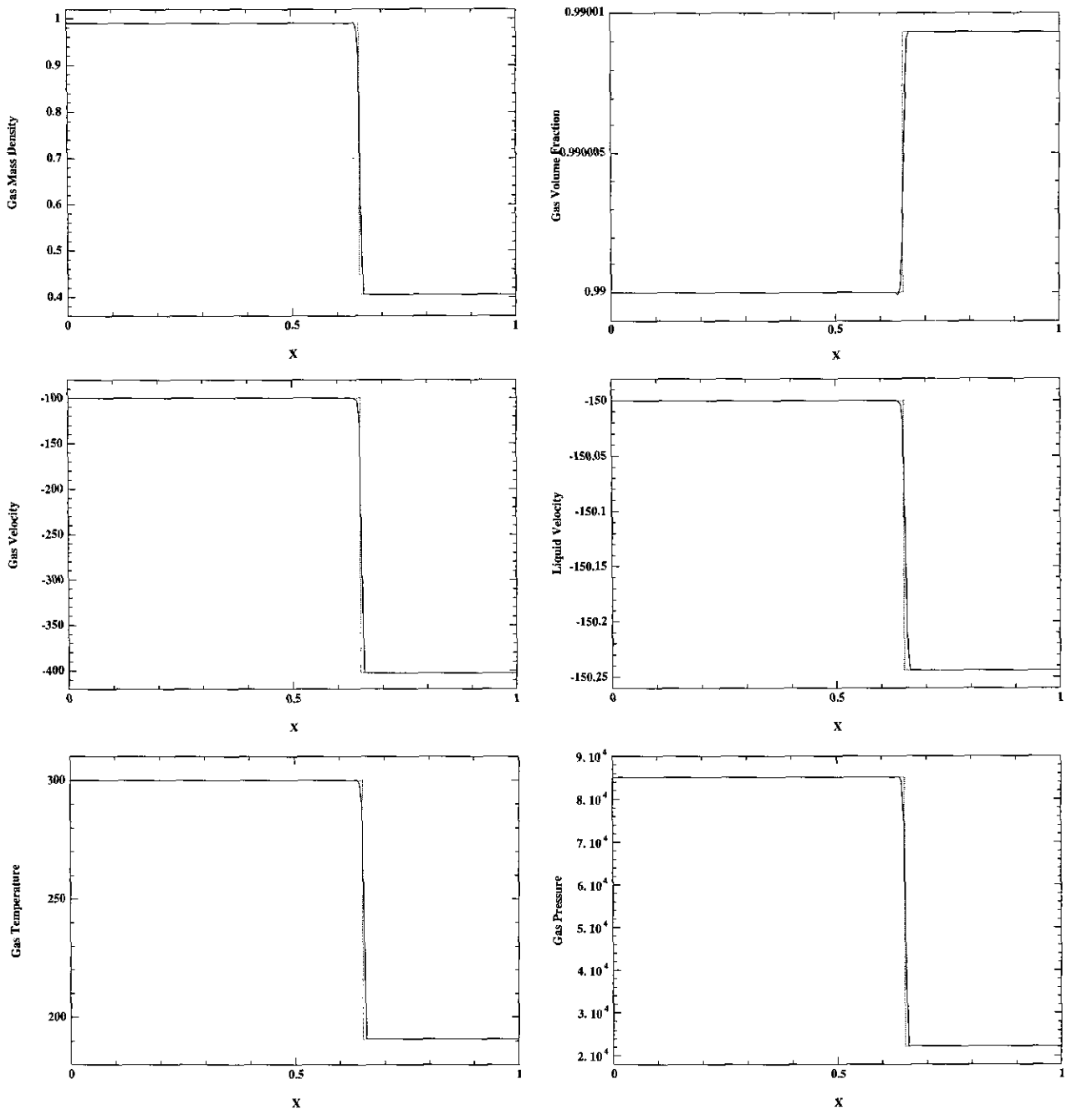

FIG. 3. Shock wave 1. Toro's method at second order, $T_0 = 5 \times 10^{-3}$ s.

$\alpha\rho_g$ and the second system consists in a simple strictly hyperbolic system. A Roe linearization of the jump conditions for this system is given by matrix $\tilde{\mathbf{A}}^0$. The obtained computer code runs very fast and is robust. The computed profiles for shock waves 1 and 2 are plotted in Figs. 7 and 8. For the first wave, the profiles of the quantities associated with the gas phase are accurately computed while the void fraction and droplets velocity profiles are miscomputed; the profiles of the liquid phase quantities are constant and equal to the right state of the initial profile. The two systems are decoupled and here the speeds of the wave solutions of (4.15.ii) all are negative and go out of the computational domain through the left boundary; inside the computational domain, the computed solution is constant and equal to the right state. Here the quantities associated with the gas phase are accurately computed since the coupling between the two phases is very small for this first example of a shock wave.

In Fig. 8 the computed profiles for the quantities associated

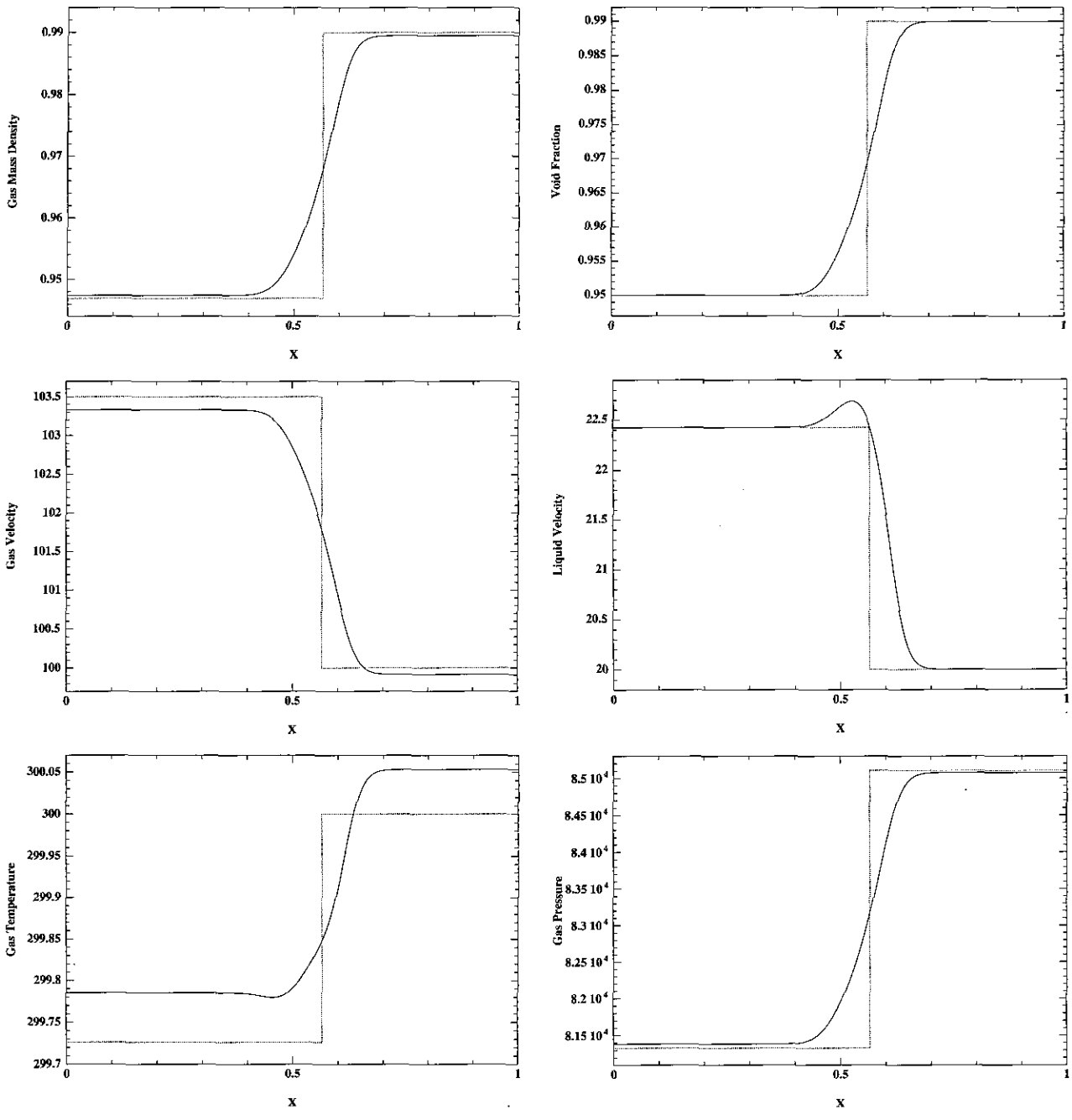

FIG. 4. Shock wave. 2. Toro's method at first order, $T_0 = 2 \times 10^{-2}$ s.

with the liquid phase are reasonable. The computed profiles are, however, made of several waves: by construction, the left and right states $\mathbf{u}^L$ and $\mathbf{u}^R$ are such that the difference $\mathbf{u}^R - \mathbf{u}^L$ is an eigenvector of matrix $\tilde{\mathbf{A}}(\mathbf{u}^L, \mathbf{u}^R)$. Here, omitting the coupling between the two phases, we only consider the eigenvectors of matrix $\tilde{\mathbf{A}}^0$: $\mathbf{u}^R - \mathbf{u}^L$ is no longer an eigenvector of this latter matrix but has a nonzero component on every eigenvector of $\mathbf{A}^0$. Hence the computed solution is composed of several waves and not the expected single wave. However, the obtained wave pattern is stable in time, unlike what happens with Toro's method.

5. TWO-DIMENSIONAL SOLVER

In two dimensions, the system we study is written

$$\partial_t(\alpha\rho_g) + \partial_x(\alpha\rho_g u_g) + \partial_y(\alpha\rho_g v_g) = 0 \qquad (5.1.i)$$

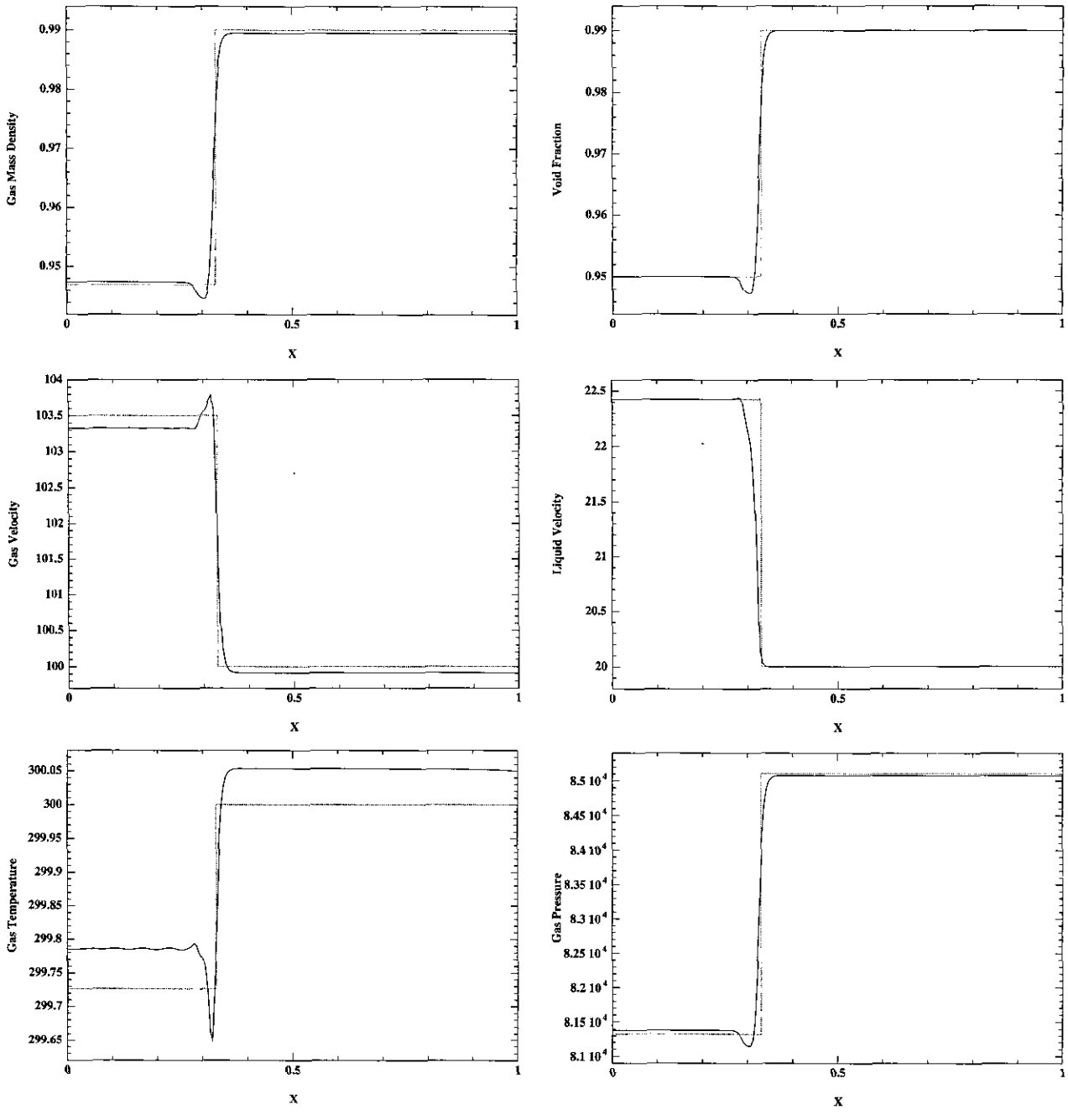

FIG. 5. Shock wave 2. Toro's method at second order, $T_0 = 2 \times 10^{-2}$ s.

$$\partial_t(\alpha\rho_g u_g) + \partial_x(\alpha\rho_g u_g^2) + \partial_y(\alpha\rho_g v_g) + \alpha\partial_x p = 0 \tag{5.1.ii}$$

$$\partial_t(\alpha\rho_g v_g) + \partial_x(\alpha\rho_g u_g v_g) + \partial_y(\alpha\rho_g v_g^2) + \alpha\partial_y p = 0 \tag{5.1.iii}$$

$$\partial_t(\alpha\rho_g e_g) + \partial_x(\alpha\rho_g e_g u_g) + \partial_y(\alpha\rho_g e_g v_g) + \partial_x(\alpha p u_g) + \partial_y(\alpha p v_g) + p\partial_x((1-\alpha)u_l) + p\partial_y((1-\alpha)v_l) = 0 \tag{5.1.iv}$$

$$\partial_t((1-\alpha)\rho_l) + \partial_x((1-\alpha)\rho_l u_l) + \partial_y((1-\alpha)\rho_l v_l) = 0 \tag{5.1.v}$$

$$\partial_t((1-\alpha)\rho_l u_l) + \partial_x((1-\alpha)\rho_l u_l^2) + \partial_y((1-\alpha)u_l v_l) + \partial_x(\theta_0(1-\alpha)^\delta) + (1-\alpha)\partial_x p = 0 \tag{5.1.vi}$$

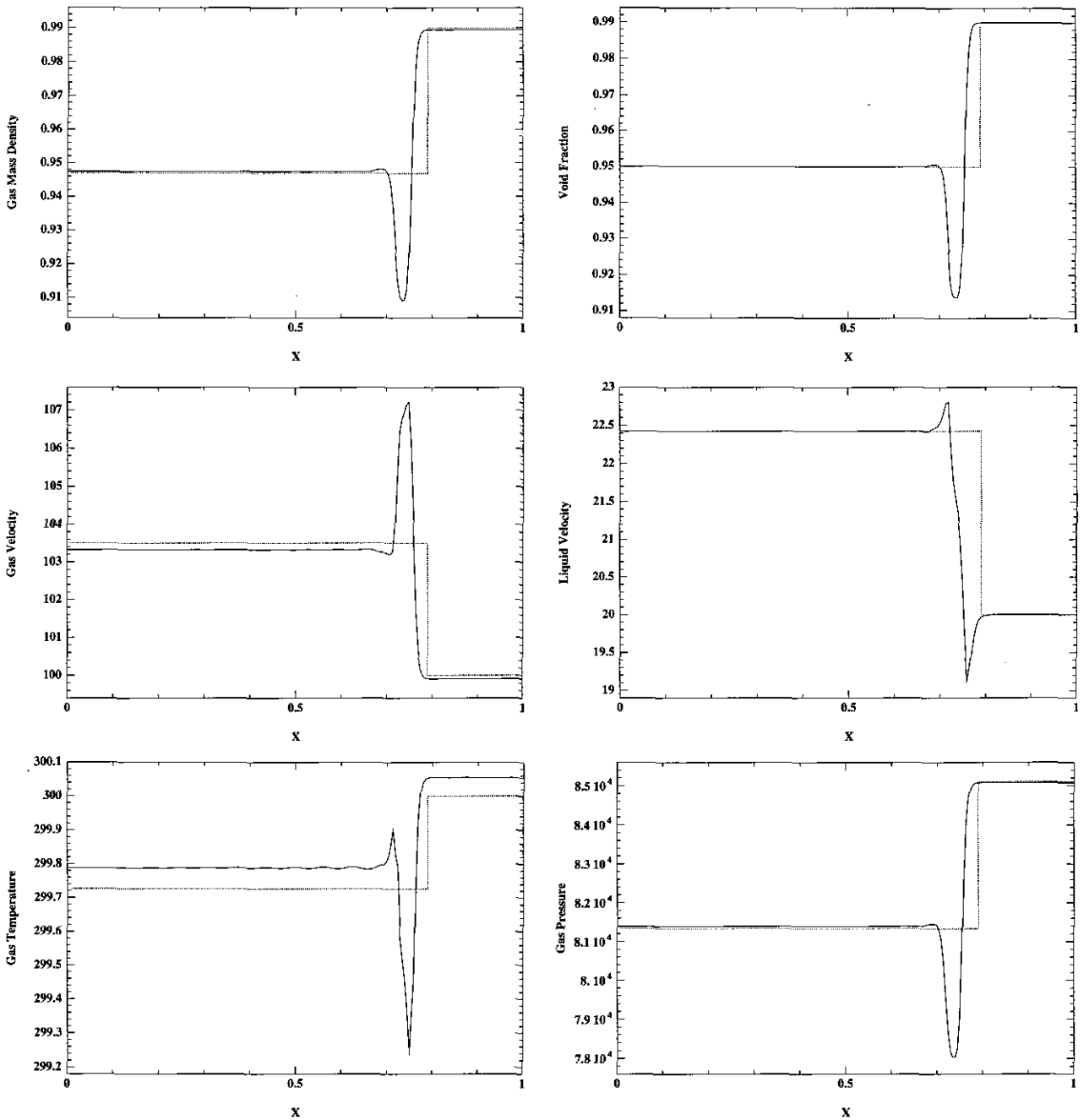

FIG. 6. Shock wave 2. Toro's method at second order, $T_0 = 3 \times 10^{-2}$ s.

$$\partial_t((1-\alpha)\rho_l v_l) + \partial_x((1-\alpha)\rho_l u_l v_l) + \partial_y((1-\alpha)v_l^2) + \partial_y(\theta_0(1-\alpha)^\delta) + (1-\alpha)\partial_y p = 0 \qquad (5.1.\text{vii})$$

$$\partial_t((1-\alpha)\rho_l e_l) + \partial_x((1-\alpha)\rho_l e_l u_l) + \partial_y((1-\alpha)\rho_l e_l v_l) + \partial_x(\theta_0(1-\alpha)^\delta u_l) + \partial_y(\theta_0(1-\alpha)^\delta v_l) + (1-\alpha)u_l\partial_x p + (1-\alpha)v_l\partial_y p = 0, \qquad (5.1.\text{viii})$$

where $e_g = \varepsilon_g + (u_g^2 + v_g^2)/2$ and $e_l = \varepsilon_l + (u_l^2 + v_l^2)/2$. We have denoted by u_g and v_g (resp. u_l and v_l) the x and y components of the gas (resp. liquid) phase velocity. To begin with, we follow [12] to write a first-order two-dimensional numerical scheme for system (5.1). Given a grid made of polygons, we construct an approximate solution $\mathbf{u}^n$ of (5.1) for each date $t_n = n\Delta t$ with $\mathbf{u}^n_{|K} = \mathbf{u}^n_K$ constant over every cell K of the grid by

$$\mathbf{u}_K^{n+1} = \mathbf{u}_K^n - \frac{\Delta t}{|K|} \sum_{A \subset \partial K} |A| \phi_{\nu_{K,A}}(\mathbf{u}_K^n, \mathbf{u}_{K,A}^n), \qquad (5.2)$$

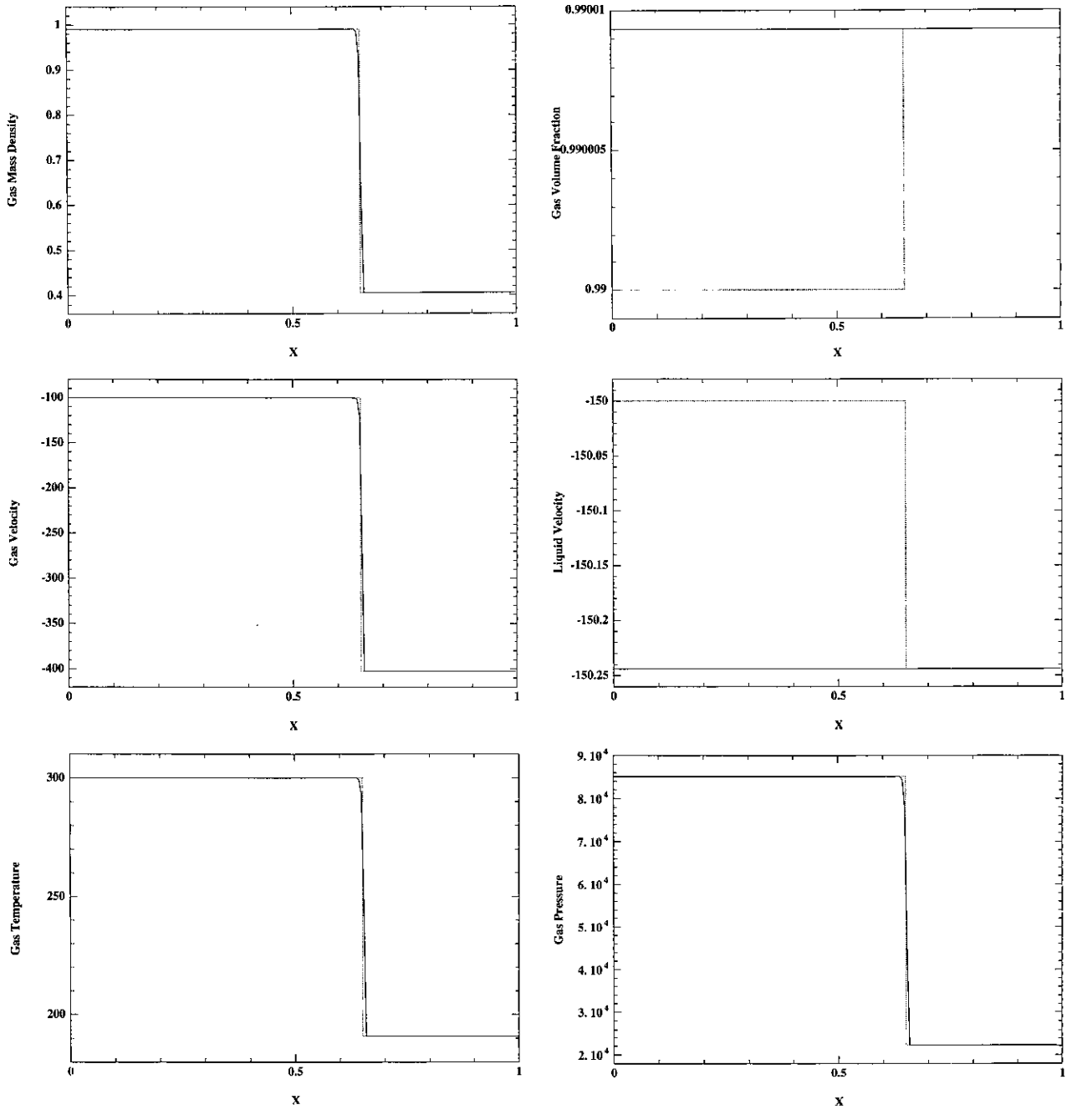

FIG. 7. Shock wave 1. Method 3 at second order, $T_0 = 5 \times 10^{-3}$ s.

where K denotes a given cell, A is one edge of K, $\nu_{K,A}$ is the outward unit normal to A, $\mathbf{u}^n_{K,A}$ is the value of the function $\mathbf{u}^n$ on the polygon neighboring K with common edge A, and $\phi_{\nu_{K,A}}$ is a numerical approximation of the flux crossing the edge A. The sum in (5.2) is performed on the different edges of polygon K.

To compute an approximation of the flux crossing the edge between two cells, we use the rotational invariance of system (5.1) (see [13] for more details.) Writing system (5.1) in the normal (ξ) and tangential (ζ) directions to a given edge A, we reduce the problem to the computation of a flux for the one-dimensional system:

$$\partial_t(\alpha\rho_g) + \partial_\xi(\alpha\rho_g U_g) = 0 \qquad (5.3.\text{i})$$

$$\partial_t(\alpha\rho_g U_g) + \partial_\xi(\alpha\rho_g U_g^2) + \alpha\partial_\xi(p) = 0 \qquad (5.3.\text{ii})$$

$$\partial_t(\alpha\rho_g V_g) + \partial_\xi(\alpha\rho_g U_g V_g) = 0 \qquad (5.3.\text{iii})$$

$$\partial_t(\alpha\rho_g e_g) + \partial_\xi(\alpha\rho_g e_g U_g) + \partial_\xi(\alpha p U_g)$$

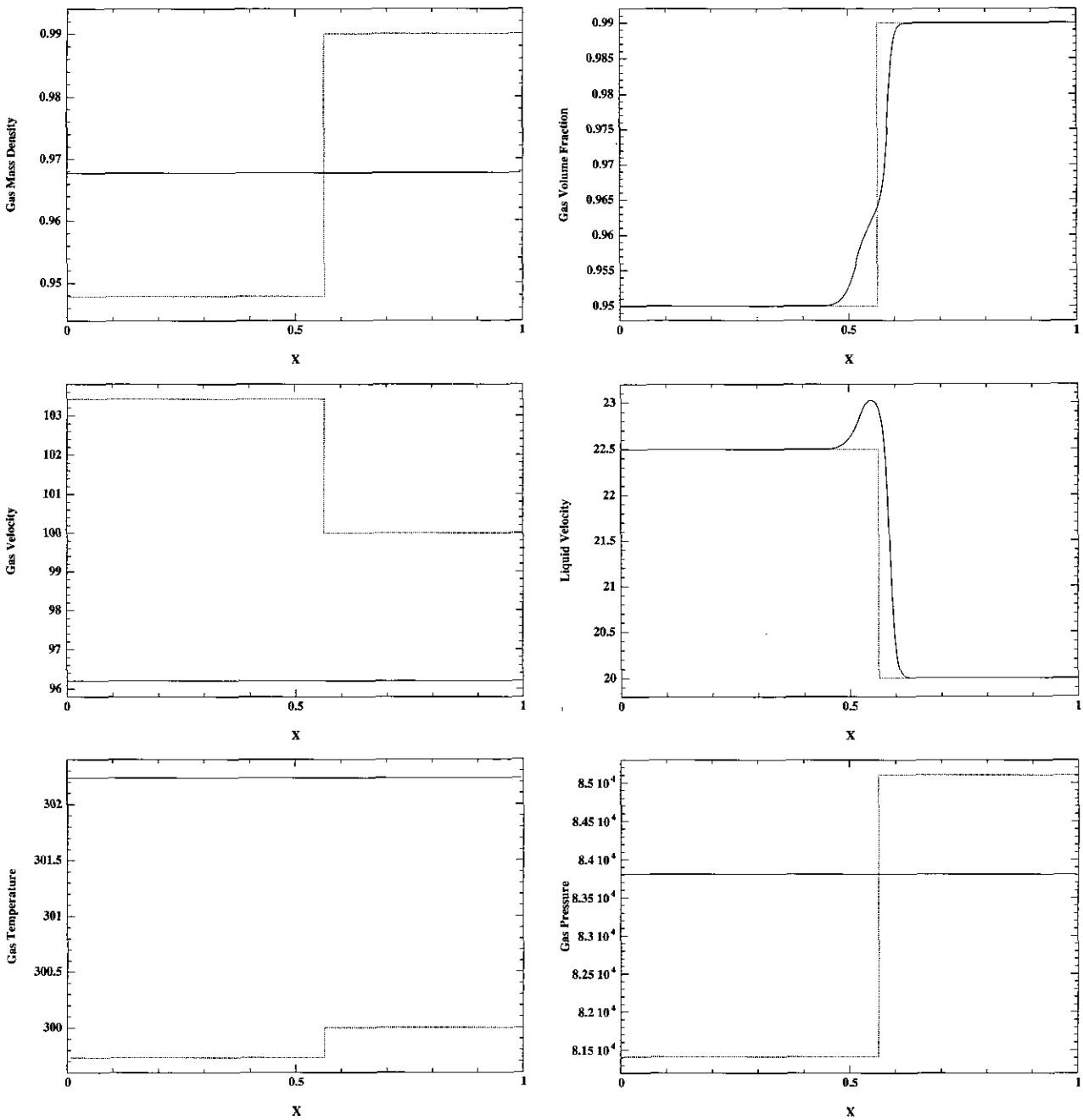

FIG. 8. Shock wave 2. Method 3 at second order, $T_0 = 2 \times 10^{-2}$ s.

$$+ p\partial_\xi((1-\alpha)U_l) = 0 \quad (5.3.\text{iv})$$

$$\partial_t((1-\alpha)\rho_l) + \partial_\xi((1-\alpha)\rho_l U_l) = 0 \quad (5.3.\text{v})$$

$$\partial_t((1-\alpha)U_l) + \partial_\xi((1-\alpha)\rho_l U_l^2) + \partial_\xi(\theta_0(1-\alpha)^\delta) + (1-\alpha)\partial_\xi p = 0 \quad (5.3.\text{vi})$$

$$\partial_t((1-\alpha)\rho_l V_l) + \partial_\xi((1-\alpha)\rho_l U_l V_l) = 0 \quad (5.3.\text{vii})$$

$$\partial_t((1-\alpha)\rho_l e_l) + \partial_\xi((1-\alpha)\rho_l e_l U_l) + \partial_\xi(\theta_0(1-\alpha)^\delta U_l) + (1-\alpha)U_l\partial_\xi p = 0, \quad (5.3.\text{viii})$$

where we have denoted by U_g and V_g (resp. U_l and V_l) the components of the gas (resp. liquid) phase velocity in the system of coordinates (ξ, ζ). This system is the same as (1.3) with the additional variables V_g and V_l. The two new characteristic fields are linearly degenerated while the other ones can be deduced from the fields of system (1.3) by simple transformations. Following the method developed in Sections 3 and 4, we write the flux $\phi_{\nu_K,A}$ crossing the edge A of the cell K in direction ν_K under the form

$$\phi_{\nu_K,A}(\mathbf{u}_K, \mathbf{u}_{K,A}) = (\tilde{\mathbf{A}}(\mathbf{z}_K, \mathbf{z}_{K,A}))^-(\mathbf{z}_{K,A} - \mathbf{z}_K), \quad (5.4)$$

where $\tilde{\mathbf{A}}$ is a Roe linearization of some correct jump conditions for system (5.3) and $\mathbf{z}$ denotes the state $\mathbf{u}$ written in the system of coordinates (ξ, ζ). The computations are no more complicated than the one in Section 4, leading to a first-order numerical scheme for solving system (5.1)

As usual when using a Roe-type Riemann solver, some nonphysical solution may appear in rarefactions and we have to use an entropy fix to correct the computed solutions. We have used either a Harten entropy fix (see [14], for instance) or a nonparametrized entropy fix described in [15, 16]. We had many difficulties determining appropriate truncation velocities for a Harten entropy fix; we chose a first truncation velocity for the genuinely nonlinear fields $\mathbf{r}_1$, $\mathbf{r}_2$ associated with gas dynamics and another one for the fields $\mathbf{r}_3$ and $\mathbf{r}_4$ associated with void fraction waves. This solution is not really satisfactory since these parameters depend on the computation to be performed. Instead we prefer to use the nonparametrized entropy fix introduced in [15, 16] which gives good results and is simple to implement.

To obtain a second-order accurate scheme, we construct for each date t_n a function $\mathbf{u}^n$ whose restriction to a given cell K of the triangulation is afine. This function may be discontinuous when crossing an edge of the grid.

Let be given at time $t_n = n\Delta t$ an approximate solution $\mathbf{u}^n$ of system (5.1). For each cell K of the grid, we set

$$\mathbf{u}_K^n = \frac{1}{|K|}\int_K \mathbf{u}^n(x)\,dx. \tag{5.5}$$

We compute next an average value of the function $\mathbf{u}^n$ at the center of an edge A between the two cells K and K_A to be

$$\mathbf{u}_A^{n+1/2} = \mathbf{W}(\mathbf{u}_K^n, \mathbf{u}_{K_A}^n), \tag{5.6}$$

where $\mathbf{W}(\mathbf{u}^L, \mathbf{u}^R)$ denotes the Roe average defined by (3.2). We introduce a function $\tilde{\mathbf{u}}^n$ that is afine in each cell K

$$\forall K, \forall (x,y) \in K, \quad \tilde{\mathbf{u}}^n(x) = \mathbf{u}_K^n + (x - x_K)\tilde{\mathbf{p}}_K + (y - y_K)\tilde{\mathbf{q}}_K, \tag{5.7}$$

where (x_K, y_K) denotes the barycenter of the cell K. When the function $\tilde{\mathbf{u}}^n$ is defined by (5.7), the slopes $\tilde{\mathbf{p}}_K$ and $\tilde{\mathbf{q}}_K$ are given by

$$\tilde{\mathbf{p}}_K = \frac{1}{|K|}\int_K \partial_x \tilde{\mathbf{u}}^n\,dx\,dy = \frac{1}{|K|}\int_{\partial K} \tilde{\mathbf{u}}^n \nu^x\,ds$$

$$\tilde{\mathbf{q}}_K = \frac{1}{|K|}\int_K \partial_y \tilde{\mathbf{u}}^n\,dx\,dy = \frac{1}{|K|}\int_{\partial K} \tilde{\mathbf{u}}^n \nu^y\,ds,$$

where $\nu = (\nu^x, \nu^y)$ is the outward normal to K. Hence we predict some slopes $\tilde{\mathbf{p}}_K$ and $\tilde{\mathbf{q}}_K$ with the formulae

$$\tilde{\mathbf{p}}_K = \frac{1}{|K|}\sum_{A\in\partial K} |A|\mathbf{u}_A^{n+1/2}\nu^x \tag{5.8.i}$$

$$\tilde{\mathbf{q}}_K = \frac{1}{|K|}\sum_{A\in\partial K} |A|\mathbf{u}_A^{n+1/2}\nu^y. \tag{5.8.ii}$$

The next stage consists in correcting the above slopes so that no oscillations appear at the interfaces between the cells of the gridding. This correction is performed on each component of the vectors $\mathbf{p}_K$ and $\mathbf{q}_K$. To this end, we replace the slopes $\tilde{\mathbf{p}}_{K,i}$ and $\tilde{\mathbf{q}}_{K,i}$ computed above by the slopes:

$$\mathbf{p}_{K,i} = \beta_{K,i}\tilde{\mathbf{p}}_{K,i}, \quad \mathbf{q}_{K,i} = \beta_{K,i}\tilde{\mathbf{q}}_{K,i}, \tag{5.9}$$

where the limiters $\beta_{K,i}$ are computed as follows: we first set

$$\tilde{\mathbf{u}}_{K,i}^M = \sup_{(x,y)\in K} \tilde{\mathbf{u}}_{K,i}(x,y), \quad \tilde{\mathbf{u}}_{K,i}^m = \inf_{(x,y)\in K} \tilde{\mathbf{u}}_{K,i}(x,y), \tag{5.10.i}$$

$$\mathbf{u}_{K,i}^M = \max_{A\in\partial K} \mathbf{u}_{K_A,i}^n, \qquad \mathbf{u}_{K,i}^m = \min_{A\in\partial K} \mathbf{u}_{K_A,i}^n. \tag{5.10.ii}$$

We set next

$$\beta_{K,i}^M = \max\left(0, \frac{\mathbf{u}_{K,i}^M - \mathbf{u}_{K,i}^n}{\tilde{\mathbf{u}}_{K,i}^M - \mathbf{u}_{K,i}^n}\right), \quad \beta_{K,i}^m = \min\left(0, \frac{\mathbf{u}_{K,i}^m - \mathbf{u}_{K,i}^n}{\tilde{\mathbf{u}}_{K,i}^m - \mathbf{u}_{K,i}^n}\right), \tag{5.10.iii}$$

and, finally,

$$\beta_{K,i} = \min(1, \beta_{K,i}^M, \beta_{K,i}^m). \tag{5.11}$$

After correction of the slopes, the approximation $\mathbf{u}^n$ we choose is

$$\forall K, \forall (x,y) \in K, \quad \tilde{\mathbf{u}}^n(x) = \mathbf{u}_K^n + (x - x_K)\mathbf{p}_K + (y - y_K)\mathbf{q}_K. \tag{5.12}$$

We can now proceed to the time iteration, following what was done in Section 3 for one-dimensional slab geometry. The increment of the average value $\mathbf{u}_K^n$ of the function $\mathbf{u}^n$ in the cell K arises from the fluxes due to the discontinuities of the function $\tilde{\mathbf{u}}^n$ at the boundary of the cell K and from the slopes of the function $\tilde{\mathbf{u}}^n$ inside the cell K. The fluxes due to the discontinuities of the function $\tilde{\mathbf{u}}^n$ at the boundaries of the cell K are computed as follows: we denote by $\tilde{\mathbf{u}}_{K,A}^{n+1/2}$ the left value of the function $\tilde{\mathbf{u}}$ defined by (5.12) at the center of the edge A,

$$\tilde{\mathbf{u}}_{K,A}^{n+1/2} = \mathbf{u}_K^n + (x_A - x_K)\mathbf{p}_K + (y_A - y_K)\mathbf{q}_K, \tag{5.13}$$

where (x_A, y_A) are the coordinates of the barycenter of A. Then these fluxes are

$$\mathbf{F}_1 = -\frac{\Delta t}{|K|}\sum_{K\in\partial K} |A|\phi_{\nu_K,A}(\tilde{\mathbf{u}}_{K,A}^{n+1/2}, \tilde{\mathbf{u}}_{K_A,A}^{n+1/2}), \tag{5.14}$$

where $\phi_{\nu_K,A}$ denotes the one-dimensional, first-order accurate numerical flux (5.4) in the direction ν_K normal to the edge A.

We compute next the increment due to the slopes of the function $\tilde{\mathbf{u}}^n$ in cell K. Consider first the case of a system of conservation laws for two flux functions $\mathbf{f}$ and $\mathbf{g}$,

$$\partial_t \mathbf{u} + \partial_x \mathbf{f}(\mathbf{u}) + \partial_y \mathbf{g}(\mathbf{u}) = 0. \tag{5.15}$$

Let K be a given cell and assume that the function $\mathbf{u}$ is continuous over K. The integration of (5.15) over $K \times [t, t + \Delta t]$ gives

$$\begin{aligned} &\frac{1}{|K|}\int_K \mathbf{u}(x, y, t + \Delta t)\, dx\, dy - \frac{1}{|K|}\int_K \mathbf{u}(x, y, t)\, dx\, dy \\ &\quad = -\frac{\Delta t}{|K|}\int_K \partial_x \mathbf{f}(\mathbf{u})\, dx\, dy - \frac{\Delta t}{|K|}\int_K \partial_y \mathbf{f}(\mathbf{u})\, dx\, dy \\ &\quad = -\frac{\Delta t}{|K|}\int_{\partial K} (\mathbf{f}(\mathbf{u})\nu^x + \mathbf{g}(\mathbf{u})\nu^y)\, ds. \end{aligned} \tag{5.16}$$

We discretize the latter expression according to

$$\mathbf{u}_K^{n+1} - \mathbf{u}_K^n = -\frac{\Delta t}{|K|}\sum_{A\in\partial K} |A|(\mathbf{f}(\mathbf{u}_{K,A})\nu_A^x + \mathbf{g}(\mathbf{u}_{K,A})\nu_A^y),$$

where the states $\mathbf{u}_{K,A}$, $A \in \partial K$, are the values of the function $\mathbf{u}$ at the center of the edge A of the boundary ∂K.

We extend this formula to the case of nonconservative systems; assume that instead of the flux functions $\mathbf{f}$ and $\mathbf{g}$, we know for any two physical states $\mathbf{u}^L$ and $\mathbf{u}^R$ convenient Roe linearizations $\mathbf{A}_x(\mathbf{u}^L, \mathbf{u}^R)$ and $\mathbf{A}_y(\mathbf{u}^L, \mathbf{u}^R)$ of the jump conditions in directions x and y, respectively. In the case of conservative systems, we require of course that

$$\forall \mathbf{u}^L, \mathbf{u}^R, \quad \begin{cases} \mathbf{f}(\mathbf{u}^R) - \mathbf{f}(\mathbf{u}^L) = \mathbf{A}_x(\mathbf{u}^L, \mathbf{u}^R)(\mathbf{u}^R - \mathbf{u}^L) \\ \mathbf{g}(\mathbf{u}^R) - \mathbf{f}(\mathbf{u}^L) = \mathbf{A}_y(\mathbf{u}^L, \mathbf{u}^R)(\mathbf{u}^R - \mathbf{u}^L). \end{cases} \tag{5.17}$$

Then choosing for each cell K a given edge A^0 and using the relations

$$\sum_{A\in\partial K} |A|\,\nu_A^x = 0, \quad \sum_{A\in\partial K} |A|\,\nu_A^y = 0,$$

we can replace (5.16) by the expression which coincides with (5.16) when (5.17) holds true,

$$\begin{aligned} \mathbf{u}_K^{n+1} - \mathbf{u}_K^n = &-\frac{\Delta t}{|K|}\sum_{A\in\partial K} |A|\mathbf{A}_x(\tilde{\mathbf{u}}_{K,A^0}^{n+1/2}, \tilde{\mathbf{u}}_{K,A}^{n+1/2})(\tilde{\mathbf{u}}_{K,A}^{n+1/2} - \tilde{\mathbf{u}}_{K,A^0}^{n+1/2})\,\nu_A^x \\ &-\frac{\Delta t}{|K|}\sum_{A\in\partial K} |A|\mathbf{A}_y(\tilde{\mathbf{u}}_{K,A^0}^{n+1/2}, \tilde{\mathbf{u}}_{K,A}^{n+1/2})(\tilde{\mathbf{u}}_{K,A}^{n+1/2} - \tilde{\mathbf{u}}_{K,A^0}^{n+1/2})\,\nu_A^y, \end{aligned} \tag{5.18}$$

where A^0 is a fixed edge of the boundary ∂K.

Finally, the second-order accurate two-dimensional numerical scheme reads

$$\begin{aligned} \mathbf{u}_K^{n+1} = \mathbf{u}_K^n &- \frac{\Delta t}{|K|}\sum_{A\in\partial K} |A|\phi_{\nu_K,A}(\tilde{\mathbf{u}}_{K,A}^{n+1/2}, \tilde{\mathbf{u}}_{K,A}^{n+1/2}) \\ &-\frac{\Delta t}{|K|}\sum_{A\in\partial K} |A|\mathbf{A}_x(\tilde{\mathbf{u}}_{K,A^0}^{n+1/2}, \tilde{\mathbf{u}}_{K,A}^{n+1/2})(\tilde{\mathbf{u}}_{K,A}^{n+1/2} - \tilde{\mathbf{u}}_{K,A^0}^{n+1/2})\,\nu_A^x \\ &-\frac{\Delta t}{|K|}\sum_{A\in\partial K} |A|\mathbf{A}_y(\tilde{\mathbf{u}}_{K,A^0}^{n+1/2}, \tilde{\mathbf{u}}_{K,A}^{n+1/2})(\tilde{\mathbf{u}}_{K,A}^{n+1/2} - \tilde{\mathbf{u}}_{K,A^0}^{n+1/2})\,\nu_A^y. \end{aligned} \tag{5.19}$$

6. TWO-DIMENSIONAL NUMERICAL RESULTS

We describe in this section the numerical computation in two-dimensional geometry of two-phase fluid flows composed of liquid droplets suspended in a gas phase. Obtaining a meaningful description of such flows requires us to take into account the convection processes, the mass, impulsion, and energy exchanges between the two phases and the breakup and coalescence of droplets. The convection terms are contained in system (5.1) and we gave in Section 5 a way to discretize these equations. The latter phenomena are taken into account by algebraic source terms that have to be added to the right-hand side of (5.1). Since we are mainly interested in the construction of accurate and robust methods for solving the convection processes in sprays, we restrict ourselves to the most fundamental exchange terms whose omission would lead to meaningless results; we just consider the drag force and the breakup of droplets that takes place when the relative velocity between the two phases is large. We omit the mass and energy exchanges (apart from the work of the drag force, of course) between the two phases. This latter assumption is valid, provided that the gas temperature T_g and the liquid temperature T_l are equal and below the boiling temperature of the liquid phase. (Anyway, taking into consideration the vaporization of droplets can be achieved very simply using a d^2 law, for instance; see [17].)

Following [18], we take for the drag force acting on a single droplet the expression:

$$\mathbf{f}_d = \frac{\pi}{2} C_D \rho_g r^2 |\mathbf{u}_g - \mathbf{u}_l|(\mathbf{u}_g - \mathbf{u}_l), \tag{6.1}$$

where r denotes the droplets radius and where the drag coefficient C_D is given by

$$C_D = \begin{cases} \dfrac{24}{\mathrm{Re}}\left(1 + \dfrac{1}{6}\mathrm{Re}^{2/3}\right) & \text{if } \mathrm{Re} \leq 1000 \\ 0.424 & \text{if } \mathrm{Re} \geq 1000 \end{cases} \tag{6.2}$$

and the droplets' Reynolds number Re is

$$\mathrm{Re} = \frac{2\rho_g |\mathbf{u}_g - \mathbf{u}_l| r}{\mu_g}. \tag{6.3}$$

We insert respectively in the right-hand terms of Eqs. (5.1.ii), (5.1.iii), (5.1.vi), and (5.1.vii) the source terms $\mathbf{I}_x$, $\mathbf{I}_y$, $\mathbf{J}_x$, and $\mathbf{J}_y$ given by

$$\begin{pmatrix}\mathbf{I}_x\\ \mathbf{I}_y\end{pmatrix} = -n\mathbf{f}_d, \quad \begin{pmatrix}\mathbf{J}_x\\ \mathbf{J}_y\end{pmatrix} = \frac{n\mathbf{f}_d}{(1-\alpha)\rho_l}, \tag{6.4}$$

where n denotes the droplets' number density.

We evaluate the droplet number density n by solving the equation

$$\partial_t n + \operatorname{div}(n\mathbf{u}_l) = \dot{n}_{bu}, \tag{6.5}$$

where $\dot{n}_{bu}$ stands for the production of droplets caused by droplet breakup. (We omit in this analysis droplet collisions.) When a droplet is exposed to a gas flow, the droplet may break if its Weber number We is too large. This number is defined by

$$\mathrm{We} = \frac{\rho_g|\mathbf{u}_g - \mathbf{u}_l|^2}{a(T_l)}, \tag{6.6}$$

where $\mathbf{u}_g$ and $\mathbf{u}_l$ are respectively the velocities of the gas flow and of the droplet, r is the radius of the droplet, ρ_g is the gas mass density, and a is the surface tension of the liquid–gas interface. Many experiments (see [19]) and theoretical considerations (see [20, 21]) have shown that a droplet exposed to a gas flow explodes when its Weber number is larger than a critical value We_c which depends on the properties of the interface. We took for the critical Weber number $\mathrm{We}_c = 7$. What we obtain after the breakup of a single droplet is not clear. Here we choose to use a model proposed in [22] after some simplifications to predict the mean radius of the droplets obtained after the breakup of a drop. In [22], the authors use the following formula that gives the mean radius $\bar{r}$ of the obtained droplets in a function of the radius r_1 of the original drop and of the deformation velocity $\dot{y}_1$ of the surface of the drop at the time of the breakup:

$$3\bar{r} = r_1 \Big/ \left(\frac{7}{3} + \frac{1}{8}\frac{\rho_l r_1^3}{a(T_l)}\dot{y}_1^2\right). \tag{6.7}$$

The value of the velocity of deformation of the surface of the drop can be estimated using the computations in [21]. Indeed we find after some computations that, provided the viscosity effects are small (i.e. $\mu_l^2/a(T_l)\rho_l r_1 \ll 1$, where μ_l is the liquid phase viscosity), the deformation velocity at the time of the breakup of the drop is approximately

$$\dot{y}_1 \simeq \sqrt{(a(T_l)/\rho_l r_1^3)}\, 0.1266\ \mathrm{We}. \tag{6.8}$$

Inserting this latter estimate in (6.7), we get for the mean radius of the droplets formed after the breakup of a drop with radius r and Weber number We:

$$\bar{r} = r/(7 + \tfrac{1}{160}\mathrm{We}^2). \tag{6.9}$$

Our model imposes that all drops found at a given location have the same radius. We assume that when the Weber number is larger than the critical Weber number at some given location, every drop breaks up to given smaller drops, all of them having the same radius given by (6.9). The production term in (6.5) reads

$$\dot{n}_{bu} = n\left[\left(7 + \frac{\mathrm{We}^2}{160}\right)^3 - 1\right] H(\mathrm{We} - \mathrm{We}_c), \tag{6.10}$$

where H denotes Heavyside's function. Indeed, after breakup, the volume fraction of the liquid phase remains constant. Denoting by $\bar{r}$ the radius of the drops after breakup and by $\bar{n}$ their number density, we have

$$1 - \alpha = \frac{4\pi}{3} r^3 n = \frac{4\pi}{3}\bar{r}^3\bar{n}.$$

Hence, the droplet number density has increased by

$$\bar{n} - n = \frac{r^3}{\bar{r}} n - n = \left[\left(7 + \frac{\mathrm{We}^2}{160}\right)^3 - 1\right] n.$$

In order to avoid the computed droplet number density becoming less than zero, we use some formulations that were introduced for the purpose of computational combustion in [16 or 22].

We compute the injection of a two-phase flow in a nozzle. The boundary conditions are treated by solving a Riemann problem. For each cell having an edge in the boundary of the computational domain, we introduce an extra cell, a symmetric relative to the boundary of the cell in the computational domain. When the boundary is a wall, the mass densities, energies, and droplet number density in this extra cell are the same as the one in the symmetric cell. The gas and liquid phase velocities in the extra cell are symmetric relative to the wall to the velocities in the cell of the computational domain. When the boundary corresponds to the inlet or the outlet of the nozzle, we impose the state in the extra cell: null velocity and very small pressures and temperatures at the outlet; the gas and droplets are injected at 200 ms^{-1}. The radius of droplets at the inlet is $r = 6 \times 10^{-6}$ m.

Figure 9 shows the gas mass density contours; these contours are very regular and have the same aspect as the contours obtained in the absence of droplets. Figure 10 shows next the void fraction contours in the whole computational domain and a zoom near the upper wall; we note the presence of a boundary layer. The droplets are dragged by the gas flow. However, the inertia of the droplets causes a concentration of the liquid phase in a sheet parallel to the upper wall in the region where the

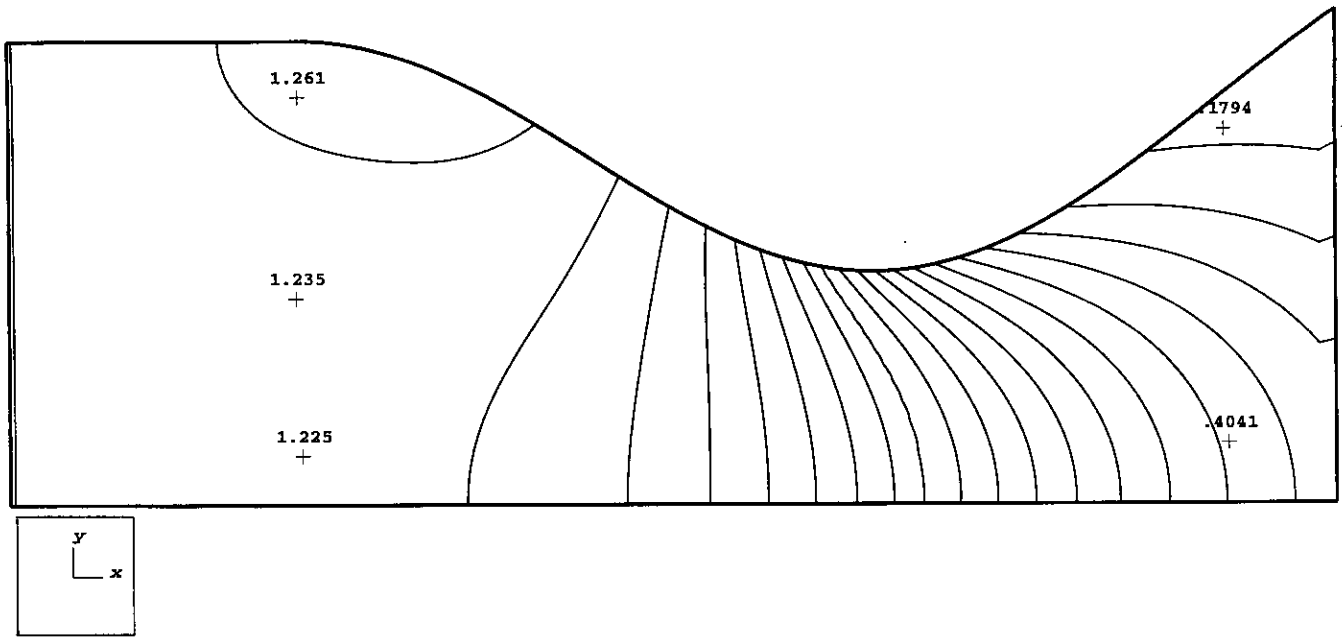

FIG. 9. Gas mass density contours.

section of the nozzle decreases. In the same manner fewer droplets are found in a layer parallel to the upper wall when the nozzle section increases. Figures 11 and 12 respectively show the gas phase and liquid phase velocity contours. In the divergent part of the nozzle, two concurrent forces determine the gas flow: the expansion of the gas tends to accelerate the flow while the droplets tends to slow this flow. Indeed the gas flow drags the droplets and accelerates the whole mass of the liquid phase. Note the boundary layer close to the upper wall in the divergent part of the nozzle; the mass density of droplets is less important in this layer so that the action of the drag force is less important. Figure 13 gives the gas temperature

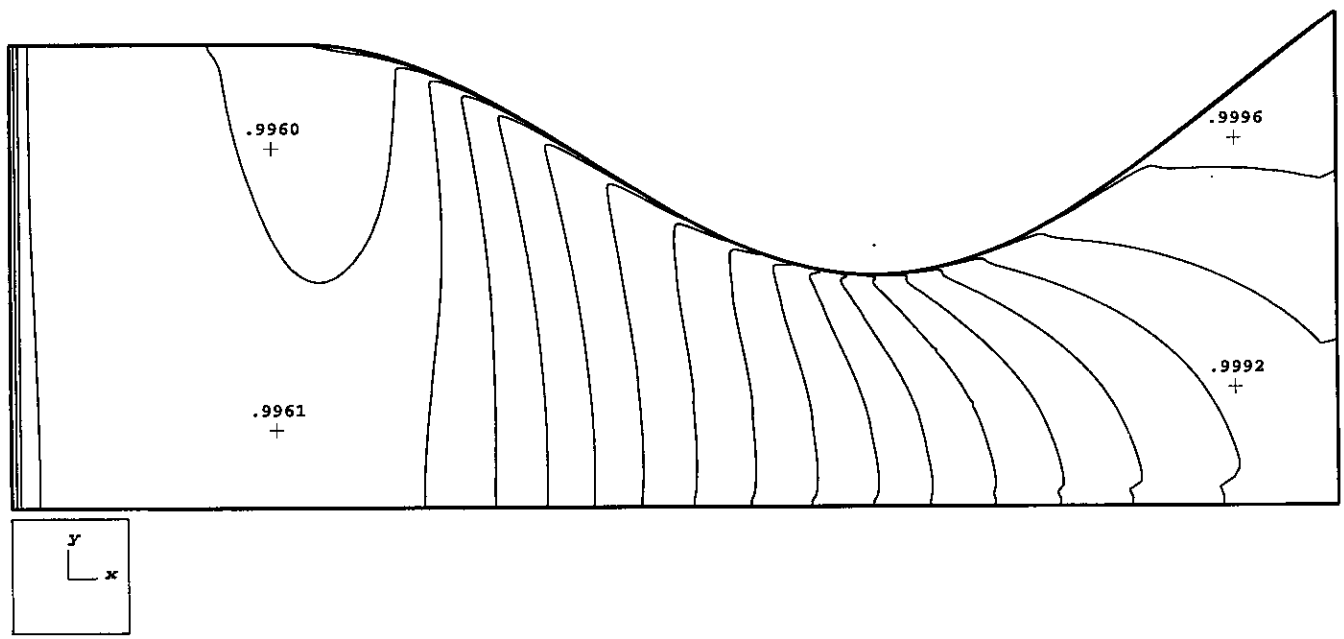

FIG. 10. Void fraction contours.

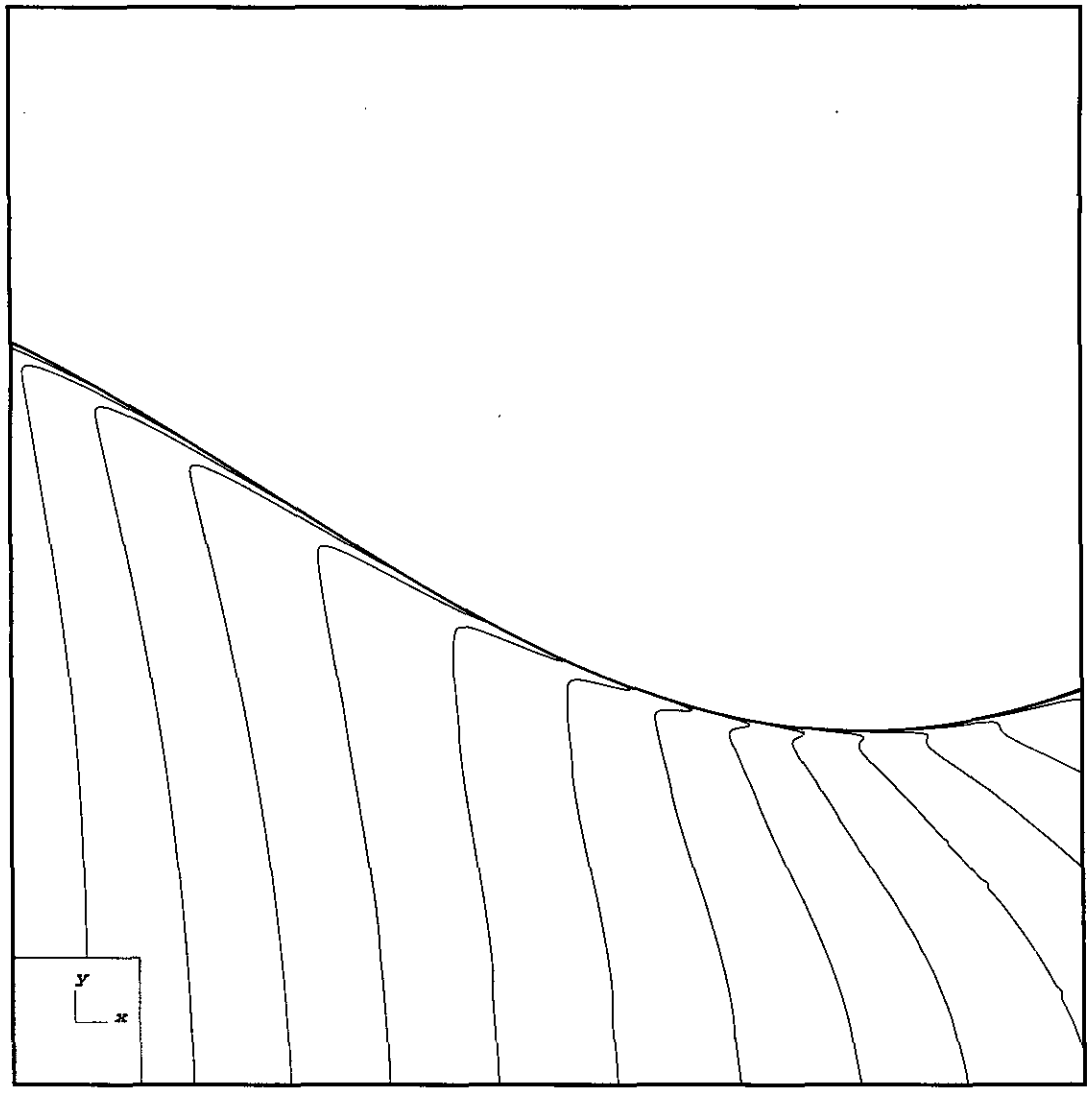

FIG. 10—*Continued*

contours. Finally, Fig. 14 gives the Mach number based on the sound velocity in the two-phase medium. Indeed, the droplets are assumed incompressible so that the compressibility of the two-phase medium is the compressibility of the gas alone. The mass density of the two-phase flow being $\rho = \alpha\rho_g + (1 - \alpha)\rho_l$, it is proven in [24] that the sound speed in the two-phase medium is written:

$$c_{\text{diph}} = \sqrt{\gamma p_g/(\alpha\rho_g + (1-\alpha)\rho_l)} = c_g \sqrt{\alpha\rho_g/(\alpha\rho_g + (1-\alpha)\rho_l)}.$$

We observe that the flow is sonic at the neck and supersonic at the outlet. This proves that the presence of the droplets fairly affects the gas flow which is slightly different from the flow of a gas in a nozzle.

The Roe-type approximate Riemann solver we constructed here gives very satisfactory results for both one-dimensional and two-dimensional computations. Its computational cost is comparable with the cost of the simplified method described in [5 or 6].

CONCLUSION

We introduced a Roe-type approximate Riemann solver for the numerical simulation of a hyperbolic system in nonconservation form modeling two-phase fluid flow. The Roe linearization matrix is obtained as a perturbation of a simple matrix whose eigenvalues and eigenvectors are explicitly known. The numerical scheme gives very satisfactory results for both 1D and 2D computations. Furthermore its computational cost is comparable with other simplified methods.

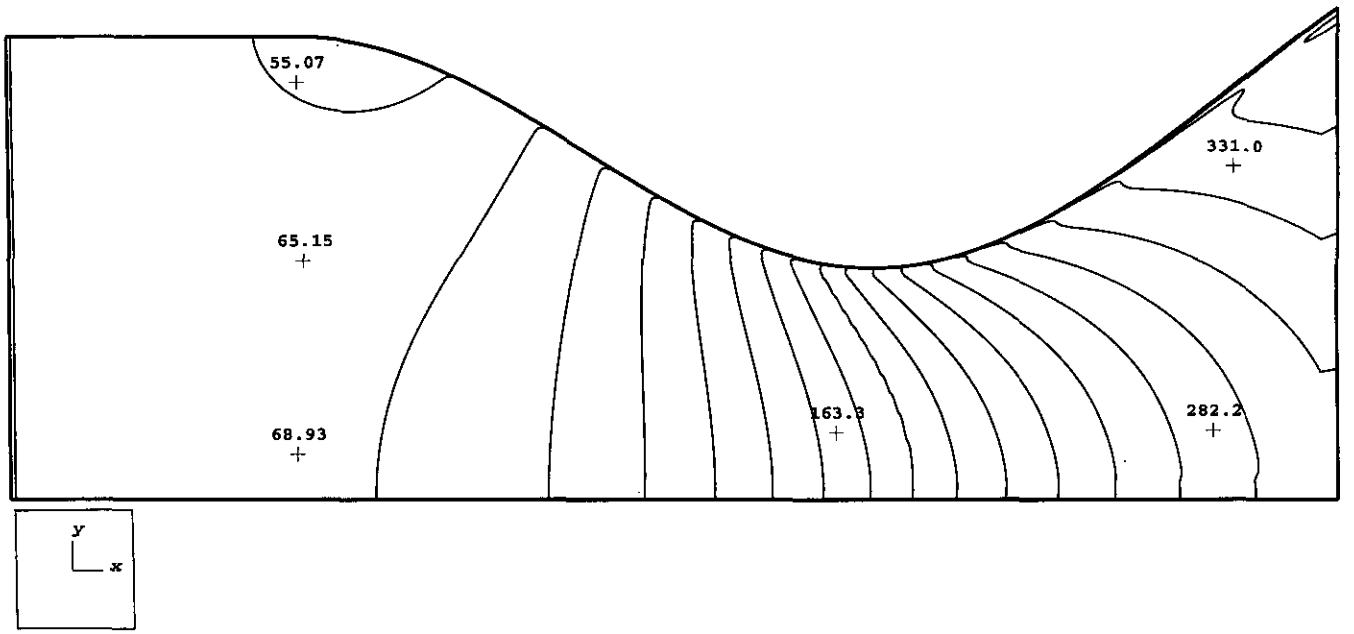

FIG. 11. Gas velocity modulus.

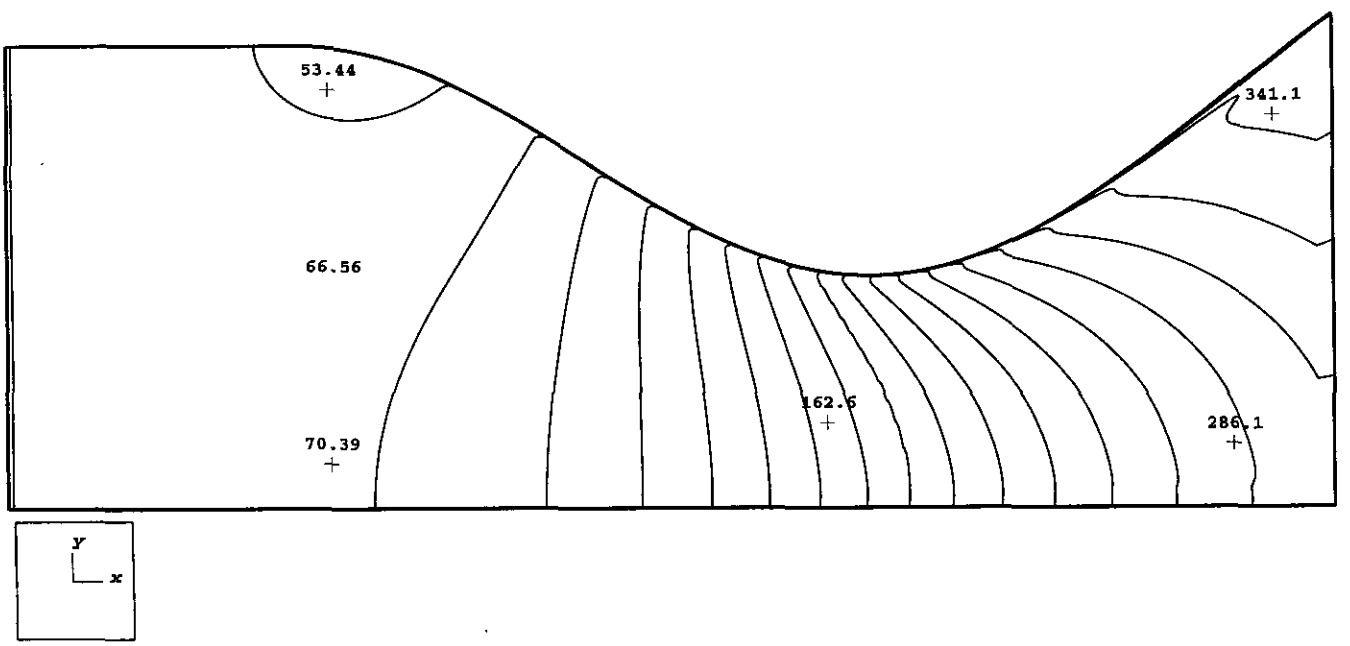

FIG. 12. Liquid phase velocity modulus.

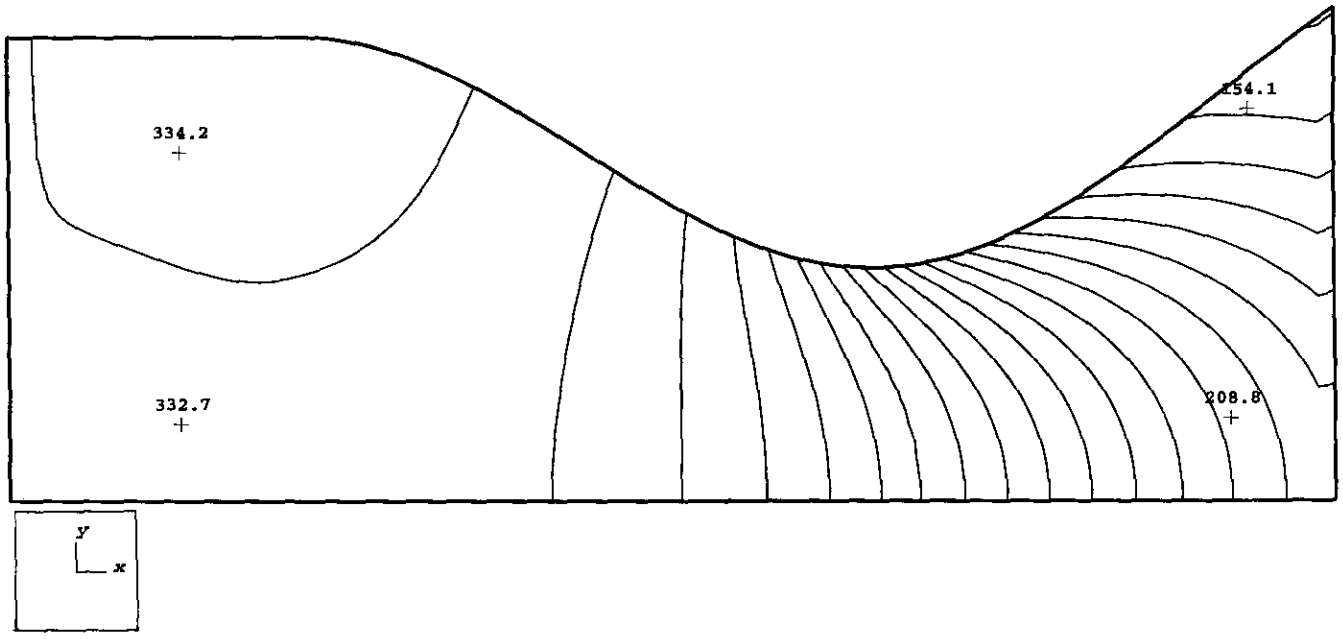

FIG. 13. Gas temperature contours.

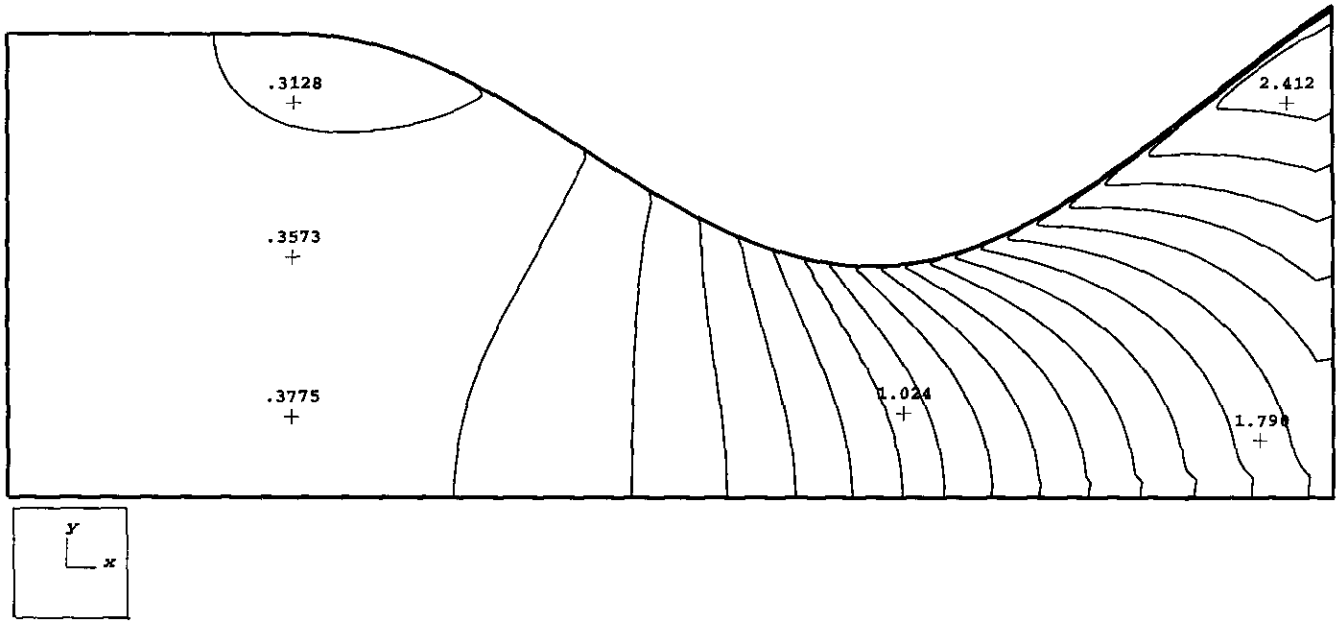

FIG. 14. Mach number.

ACKNOWLEDGMENTS

The author thanks Bernard Larrouturou for many interesting discussions in the field of the numerical simulation of two-phase flows. This work was partly supported by Société Européenne de Propulsion, Vernon, France.

REFERENCES

1. L. Sainsaulieu, "An Euler System Modeling Vaporizing Sprays," in *Dynamics of Heterogeneous Combustion and Reacting Systems,* Progress in Astronautics and Aeronautics, Vol. 152, (AIAA, Washington, DC, 1993), p. 280.
2. P.-A. Raviart and L. Sainsaulieu, *Math. Methods Models Appl. Sci.* **5**(3), 297 (1995).
3. P.-A. Raviart and L. Sainsaulieu, "Mathematical and Numerical Modeling of Two-Phase Flows," in *Computing Methods in Science and Engineering,* edited by Glowinski (Nova Science, New York, 1991), p. 119.
4. L. Sainsaulieu, in preparation.
5. E. F. Toro, "Riemann-Problem Based Techniques for Computing Reactive Two-Phase Flows," in *Numerical Combustion,* edited by Dervieux and Larrouturou, Lect. Notes in Physics, Vol. 351 (Springer-Verlag, Heidelberg, 1989), p. 472.
6. L. Sainsaulieu and B. Larrouturou, Report CERMICS, 1992 (unpublished).
7. D. Wagner, *SIAM J. Math. Anal.* **20**(5), 1035 (1989).
8. L. Sainsaulieu, *SIAM J. Appl. Math.,* to appear.
9. P. L. Roe, *J. Comput. Phys.* **43,** 357 (1981).
10. I. Toumi, *J. Comput. Phys.* **102,** 360 (1992).
11. B. Van Leer, *J. Comput. Phys.* **23,** 263 (1977).
12. F. Jouve and P. Le Floch, private communication.
13. B. Larrouturou, Report CERMICS, to appear.
14. E. Godlewski and P.-A. Raviart, "Hyberbolic Systems of Conservation Laws" (Ellipses, Paris, 1991).
15. F. Dubois and G. Mehlman, *SIAM J. Num. Anal.,* submitted.
16. G. Mehlman, Ph.D. thesis, Ecole Polytechnique, 1991 (unpublished).
17. F. A. Williams, *Combustion Theory,* 2nd ed. (Benjamin Cummings, New York, 1985).
18. P. J. O'Rourke, Ph.D. thesis 1532-T, Princeton University, August 1981 (unpublished).
19. A. Wierzba and K. Takayama, *Rep. Inst. High Speed Mech.* **53**(382), 1 (1987).
20. J. O. Hinze, *Appl. Sci. Res. A* **1,** 263 (1948).
21. J. O. Hinze, *Appl. Sci. Res. A* **1,** 273 (1948).
22. A. A. Amsden, P. J. O'Rourke, and T. D. Butler, Los Alamos Report LA-11560-MS, May 1989 (unpublished).
23. B. Larrouturou, *J. Comput. Phys.* **95**(1), 59 (1991).
24. F. Bereux, *Comput. Methods Appl. Mech. Eng.,* to appear.